NASA Technical Memorandum 73257

An Experimental Investigation of Boundary Layer and Crossflow Characteristics of the Ames 2- by 2-Foot and 11- by 11-Foot Transonic Wind-Tunnel Walls

Gerald E. Matyk and Yasunori Kobayashi

DECEMBER 1977

NASA

NASA Technical Memorandum 73257

An Experimental Investigation of Boundary Layer and Crossflow Characteristics of the Ames 2- by 2-Foot and 11- by 11-Foot Transonic Wind-Tunnel Walls

Gerald E. Matyk and Yasunori Kobayashi
Ames Research Center
Moffett Field, California

National Aeronautics
and Space Administration

**Scientific and Technical
Information Office**

1977

NOMENCLATURE

M_∞	free-stream Mach number
p	pressure, N/m^2
q	dynamic pressure, N/m^2
R	porosity parameter
Re	Reynolds number
T	temperature, K
v,V	velocity, m/sec
$\bar{V}$	mean crossflow velocity, m/sec
$\bar{v}'$	fluctuating component of crossflow velocity, m/sec
β	$\sqrt{1 - M_\infty^2}$
Δ	incremental change in quantity following, as in Δp
δ^*	displacement thickness, m
ρ	density, kg/m^3

Subscript

c	plenum chamber
s	surface of wall model
y	direction normal to wall models
∞	free stream
$\dagger$	total

AN EXPERIMENTAL INVESTIGATION OF BOUNDARY LAYER AND CROSSFLOW CHARACTERISTICS OF THE AMES 2- BY 2-FOOT AND 11- BY 11-FOOT TRANSONIC WIND-TUNNEL WALLS

Gerald E. Matyk* and Yasunori Kobayashi*

Ames Research Center

SUMMARY

An experimental investigation of the boundary layer and crossflow characteristics of the Ames 2- by 2-Foot and 11- by 11-Foot Transonic Wind-Tunnel wall configurations has been performed for Mach numbers ranging from 0.5 to 1.2 and for various crossflow to free-stream unit mass-flow ratios $(\rho v)_y/(\rho u)_\infty$.

For the 2- by 2-ft and 11- by 11-ft wall configurations, these ratios ranged from 0 to 0.12 and from 0 to 0.07, respectively. Most notably, for both wall configurations, the pressure-drop coefficient across the wall was nonlinear with mass flow and invariant with Mach number.

INTRODUCTION

A most difficult and continuing problem in wind-tunnel testing is that of correcting for the wall-interference effects. Theoretical analyses of average boundary conditions representing a partly opened surface have been developed by many authors. These analyses are based on the concept of an equivalent homogeneous-boundary close to the actual wall, and on the assumptions of potential flow and small velocity perturbations near the wall (refs. 1 through 5). But these theoretical models are sometimes unrealistic for practical flowfield conditions, even when the effects of viscosity are known from experiment (ref. 6). Some nonlinear inviscid treatments of the flow near the surface have been proposed in the case of a simple slotted wall (ref. 7) as an improvement over the linear theory. In reference 8, corrections for lift and blockage interference are established for porous tunnels of various cross-sectional shapes, and for both two- and three-dimensional flows. These theoretical results, however, need to be evaluated further by experimental evidence before they are used generally in wind-tunnel testing.

On the other hand, numerous experiments have been conducted to develop optimum slot or porosity distributions for designing minimum interference tunnel-wall configurations. Most of these studies have concentrated on

---

*National Research Council Postdoctoral Research Associate.

wall-interference effects on the flowfield around, and forces on, the model installed in the center of the test section. These experimental results have made a general contribution to the development and improvement of testing in transonic wind tunnels (refs. 9-11). However, there is still a need for further study of the fundamental features of flowfields near porous surfaces in order to solve the basic problems in predicting wall-interference effects. These problems include the behavior of boundary-layer flows and their effect on crossflow characteristics, the resistance to crossflow through the wall, the existence of equivalent homogeneous boundary conditions, and shock-wave and boundary-layer interactions at the wall.

The purpose of this experiment was to perform a detailed flowfield survey near a slotted wall surface, with the intention of obtaining basic information about the boundary-layer and crossflow characteristics. Two wall configurations were chosen similar to those of the Ames 2- by 2-Foot, and 11- by 11-Foot Transonic Wind Tunnels. The final aim of this experiment was to apply the results to the modeling of the boundary condition for use in predictions of wall-interference effects in these tunnels.

EXPERIMENTAL APPARATUS AND INSTRUMENTATION

2- by 2-Foot Transonic Wind Tunnel

The experiment was conducted in the Ames 2- by 2-Foot Transonic Wind Tunnel, in the Mach number range $0.5 \leq M_\infty \leq 1.2$. The tunnel is of the variable-pressure, closed-circuit, continuous-flow type. The tunnel walls have longitudinal slots which contain crisscrossed baffle plates (fig. 1), designed to prevent flow recirculation within the slots. Throttle bars behind the slots permit a variation in the effective open area ratio of the walls from 0 to 20.8%. In the present experiment, the throttles were in the closed position so that the floor, ceiling, and one side wall were completely closed.

The other side wall consisted of a panel frame that was originally designed for the study of the influence of the turbulent boundary layer on panel flutter (ref. 12). The frame contained an opening, 0.279 by 0.508 m (11 by 20 in.) in size, within which were mounted samples of two transonic wind-tunnel walls for testing in the present experiment (fig. 2). The upstream portion of the frame consisted of a splitter plate with a sharp leading edge (fig. 2). The entire frame could be moved from a flush position with the tunnel wall to a maximum distance of 0.051 m (2 in.) into the mainstream, thereby controlling the boundary-layer thickness on the wall models.

A sealed rectangular plenum chamber 0.229 m (9 in.) wide, 0.508 m (20 in.) long, and 0.203 m (8 in.) deep was attached behind the panel opening. The chamber was connected to a suction pump by a hose containing an orifice meter. A schematic of the test apparatus is shown in figure 3, and a photograph is shown in figure 4.

Wall Models

The two rectangular wall models were machined from an aluminum alloy plate. One model was of the same geometry as the slotted walls of the 2- by 2-ft wind tunnel, with an open area ratio of 20.8% (fig. 5(a)). The other model was of the same geometry as the wall of the 11- by 11-ft wind tunnel, which has a fixed porosity of 5.6%, except that the distance between slot centers on the model was one-half that of the actual wall (fig. 5(b)). Crossflow characteristic curves, that is, plots of $\Delta p/q$ versus $(\rho v)_y/(\rho V)_\infty$, of the actual 11- by 11-ft wall geometry were obtained by taping over alternate slots of the wall model. Note that, in figure 5, the flow direction is parallel to the longitudinal axis of the slots for both wall models, but the slot length of the 11- by 11-ft model is shorter than that of the 2- by 2-ft model.

Instrumentation

A copper-constantan thermocouple was supported from the side wall of the panel plenum chamber to obtain the total temperature (fig. 3). Streamwise static pressure distributions were obtained from a survey tube that extended through the length of the test section at a distance of 0.305 m (12 in.) from the side wall. The static pressure inside the plenum chamber was measured by means of a tube extending through the back wall of the chamber (fig. 3).

A total of 18 static pressure orifices were installed in the surface of the 11- by 11-ft wall model, and 20 in the 2- by 2-ft model, to measure the surface pressure distribution. The locations of these orifices are shown in figure 6, and a photograph of the 11- by 11-ft model is shown in figure 7.

Three retractable boundary-layer total-pressure probes were used, with locations upstream of the panels, on the panel slots, and downstream of the panel slots (fig. 6). Boundary-layer displacement thicknesses were calculated using the measured total pressures, wall static pressures, and free stream total temperature.

A thin-plate orifice meter, designed according to the ASME Standard (ref. 13) for measuring mass-flow rates, was used to measure the mass flow of the air across the panels. The total temperature used in the calculations was that measured in the plenum chamber.

Another type of total pressure probe (fig. 8) was used to survey total pressure distributions across the exit of the slot in the plenum chamber. The probe tip was 0.127 mm (0.05 in.) from the slot exit, and measurements were made at three streamwise stations. However, because of the instrumentation error involved, these measurements could not be used for the calculation of crossflow velocities, as explained in the section "Crossflow Through the Slots."

A hot-wire sensor with a wire diameter of 5 μm and a length of 0.8 mm (0.0315 in.) was also mounted on the traversing mechanism for measuring mean

velocity distributions and fluctuations of crossflow behind the slot. A constant-temperature-type anemometer (DISA-55M model) was used.

At each test condition, measurements were taken with the above apparatus for various values of free-stream Mach number and crossflow to unit mass-flow ratio $(\rho v)_y/(\rho V)_\infty$. Both static and total pressures in the tunnel as well as the reference pressure, that is, the free-stream static pressure at the position of the wall model, were measured with absolute-pressure-sensing, mercury-servomanometer followers. All other pressures were connected to conventional strain-gauge-differential-type transducers. Positions of the slot probe and those of the boundary-layer probes were detected by potentiometer systems.

Maximum expected instrumentation errors in the manometer followers and pressure transducers were ± 34.5 N/m^2 (0.005 psi) and ± 138 N/m^2 (0.02 psi), respectively. The potentiometer system could locate the positions of the probes to within an error of 0.51 mm (0.02 in.).

EXPERIMENTAL RESULTS AND DISCUSSION

Boundary-Layer Characteristics of the Wall Models

Boundary-layer displacement thicknesses δ^*, calculated using the boundary-layer probe data at the three locations on the wall and the free-stream total temperatures, are given in figures 9-12. The data are presented for the 2- by 2-ft wall model and for both the taped and the untaped versions of the 11- by 11-ft model. These models had open area percentages of 20.8, 5.6, and 11.2, respectively.

In figure 9, δ^* is shown as a function of free-stream Mach number for the case of zero auxiliary suction. From probe 1 data, it can be seen that, in the Mach number range from 0.5 to 1.2, δ^* does not vary significantly upstream of the model. Likewise, from probe 2, the same is seen to be true along the solid slots. Along the slots, however, beginning approximately at $M_\infty = 0.8$, there is an increase in δ^*. This is most obvious for the 2- by 2-ft model, for which probe 3 was immediately downstream of the center slot. It is believed that this increase in δ^* is caused for the most part by an aspirating effect occurring in the plenum behind the wall model. Due to the boundary-layer buildup along the surface of the wall model, there exists a longitudinal pressure gradient whereby, for subsonic flow, the tunnel static pressure is lower at the downstream end of the models. This induces a flow from the downstream end of the model plenum into the mainstream, which in turn causes a flow in the reverse direction at the upstream end of the wall model. The outflow from the plenum naturally causes a thickening of the boundary layer at the downstream end of the models, and this effect is greatest at the higher subsonic Mach numbers. When the free-stream flow is supersonic, air is forced into the upstream end of the model plenum as a result of the high-pressure area present there due to pressure waves emanating from the "viscous ramp" at the wall. This air must exit the plenum at the downstream end, again causing a thickening of the boundary layer at that point. Thus, when little or no

auxiliary suction is applied from behind the wall model, the probe at the downstream end of the model indicates values of δ^* that cannot be attributed to the natural growth of the boundary layer along the wall. In the case of the 11- by 11-ft wall model, the shorter slot length would tend to lessen the magnitude of this effect because the pressure gradient along the model is smaller. In addition, probe 3 was considerably further downstream from the trailing edge of the slots of the 11- by 11-ft model (see fig. 6), at which point the effect would not be felt as strongly.

It can be seen from figure 9 that, for zero mass flow across the walls, δ^* is greater over the slots than over the slats. On the 2- by 2-ft wall, for example, δ^* is roughly 50% greater over the slots than over the slats at low Mach numbers, allowing for the slight difference in the axial locations of probes 2 and 3. One would expect, however, that for a fixed M_∞, the ratio of δ^* on the slot to δ^* on the slat will vary along the axis of the tunnel, since the two boundary layers will grow at different rates. Hence, these δ^* values are only representative of one axial location in the actual tunnel.

Comparing the boundary layers on the two panels at probe 2, one can see that on the 2- by 2-ft panel, δ^* has increased considerably from its value at probe 1 upstream, whereas there is essentially no change on the 11- by 11-ft panel. On the 2- by 2-ft panel, probe 2 was located at a lateral distance of 1.6 slot widths from the two adjacent slots, whereas on the 11- by 11-ft panel the corresponding distance was 3.1 slot widths. Consequently, the boundary layer at probe 2 was more strongly influenced by the slots on the former panel than on the latter. In addition to this, probe 2 was located further downstream of the leading edge of the slots of the 2- by 2-ft model, which could also account for some of the difference between the measurements on the two wall models. It is expected that, at the location of probe 2, δ^* should be the same for both the untaped and the taped versions of the 11- by 11-ft wall, since neither is affected by the adjacent slots. This is verified by comparing figure 9(b) and 9(c). Again, the lateral extent of the influence of the slots is probably a function of the length of the slots and the above discussion pertains only to a fixed longitudinal location.

Figures 10 through 12 show the effect of mass-flow removal on the boundary-layer displacement thicknesses for the three wall models. It is seen at once that the displacement thickness at probe 1 upstream of the models is unaffected by mass-flow ratios as large as 10% and does not vary with Mach number (figs. 10(a) and 11(a)). At the location of probe 2 on the model slats, there is still very little variation of δ^* with M_∞ for all mass-flow ratios. For the 2- by 2-ft panel, δ^* at probe 2 is reduced to its upstream value at approximately 2% mass flow (fig. 10(b)). For the 11- by 11-ft panel, δ^* at probe 2 is essentially the same as upstream of the panel, and there is not much reduction even at very high values ($\simeq$10%) of the mass-flow ratio (figs. 11(b) and 12). At the location of probe 3, downstream of the slots of the wall models, there appears to be considerable variation in δ^* with M_∞, but only at the lower values of $(\rho v)_y/(\rho V)_\infty$ (figs. 10(c) and 11(c)). However, as discussed above in connection with figure 9(a), these large values of δ^* are attributed in part to an aspirating effect occurring in the plenum behind the wall models; they are not indicative of the actual boundary-layer growth

along the walls. When the auxiliary suction is increased to approximately 2%, the aspirating effect is suppressed, eliminating the variation in δ^* with M_∞ at a fixed value of $(\rho v)_y/(\rho V)_\infty$. Nevertheless, it is still evident that δ^* initially decreases quite rapidly with increasing $(\rho v)_y/(\rho V)_\infty$ achieving its upstream value at an outflow ratio of approximately 2%.

The effect on the boundary layers of moving the side wall into the mainstream by 0.035 m (1-3/8 in.) is also shown in figure 10. Bypassing the side-wall boundary layer of the tunnel reduced the value of δ^* upstream of the wall models by approximately 75%, from $\delta^* = 4.06$ mm (0.16 in.) to $\delta^* = 1.02$ mm (0.04 in.) (see fig. 10(a)). Immediately downstream of the slots, however, δ^* did not change significantly because of the panel displacement (fig. 10c). Thus, probe 3 was sufficiently far downstream of the leading edge of the 2- by 2-ft wall model to be unaffected by the boundary layer of the tunnel itself. Probe 2, on the other hand, was affected since a reduction in δ^* of 40 to 50% occurs there as a result of the panel displacement (fig. 10b). This fact has a direct bearing on the ratios of δ^* on the slot to δ^* on the slat discussed previously; however, the basic trends remain the same.

Regarding all of the boundary-layer characteristics discussed above, it must be remembered that the wall models of the present investigation are not of the conventional open-slotted type. The rapid rate of growth of the boundary layer over the slots is, in particular, attributed to the geometry of the inserts in the slots. Since in an open-slotted tunnel the streamwise velocity in the slots is not zero, the boundary layer on such a wall differs from those of the present experiment. On the other hand, it is expected that a slotted wall having perforated cover plates would have boundary-layer characteristics similar to those discussed here.

Main Flowfield Static Pressure and Model Surface Pressure Distributions

Distributions of static pressure p in the free stream and model surface pressure p_s along the free-stream direction are shown in figures 13 and 14. It is seen that the static pressure in the test section of the tunnel was very uniform when the splitter plate was flush with the side wall. For $M \leq 0.85$, the deviations from the mean static pressure were on the order of 0.1%, which is about the same as the instrumentation error involved. During these measurements, the survey tube was located along the longitudinal axis of the tunnel, at lateral distances of 20 and 26 slot widths from the 11- by 11-ft and the 2- by 2-ft models, respectively.

The model surface pressures shown in figures 13 and 14 were measured at pressure taps along the slat centerlines (see figs. 6(a) and 6(b) for details). It can be seen that, for crossflow mass-flow ratios of 3 and 4%, the surface pressure distributions along the models were quite uniform and only slightly lower ($\simeq$700 N/m^2 or 0.1 psi) than the free-stream static pressure.

When the splitter plate was moved into the free stream approximately 0.05 m (2 in.), a pressure gradient occurred along the flow direction

(figs. 15 and 16). This gradient amounted to a decrease in static pressure of approximately 7% over the length of the 2- by 2-ft model at $M_\infty = 0.7$, and only 1% over the shorter 11- by 11-ft model at $M_\infty = 0.5$. Although p was not measured far enough downstream to detect the pressure recovery, calculations confirm that the pressure gradient was caused by the reduction in the cross-sectional area of the test section. As mentioned previously, the slots in the ceiling and floor of the tunnel were closed.

Surface pressures on the slats of the wall models along a line transverse to the free-stream direction are shown in figures 17 and 18. These pressures were slightly lower than the free-stream pressure and were essentially uniform. Only in the near vicinity of the slots did the values of p_s fall a few percent. However, the static pressure distributions indicate that some wavy disturbances become prominent in the transonic range, especially in the case of the 2- by 2-ft model. At $M_\infty = 1.2$, the static pressure deviation across the slat of the 2- by 2-ft model is approximately 2.5% of the mean (fig. 18).

Crossflow Through the Slots

Crossflow characteristics curves for the three wall models are presented in figures 19 through 21. Only the portions of the curves corresponding to outflow are presented, since the present investigation had no provision for blowing air from the plenum into the mainstream. Generally, the slopes of such curves are less for inflow than for outflow, that is, the tunnel walls are effectively more open to inflow than to outflow. The reason for this is, of course, that in the case of outflow, the mainstream (which has its momentum essentially parallel to the tunnel walls) must be made to turn in a direction normal to the walls. The air in the plenum, on the other hand, is basically in a state of stagnation and hence can be directed more readily through the walls.

The porosity parameter of a porous wall R is an empirical value related to the effective porosity of the walls, taking into consideration open area ratio, hole-size-to-wall-thickness ratio, boundary-layer displacement thickness, etc. In the analytical study of the average boundary conditions for perforated walls, and slotted walls with viscous effects in the slots included, the porosity parameter is defined as

$$R = 2\,\frac{(\rho v)_y/(\rho V)_\infty}{\Delta p/q_\infty}$$

For a completely closed wall, $R = 0$, whereas for a freejet, $R \to \infty$. For porous walls the assumption is made that the characteristic curve is linear, in which case the porosity parameter is obtained from its slope. However, it is well known that the characteristic curves of porous walls are nonlinear, and so one must choose a slope that most closely fits the characteristic curve in the regions of outflow and inflow corresponding to the actual conditions in the tunnel during testing. Thus, there exists the need to measure the local pressures along the tunnel walls during model tests and then to choose

from this a "weighted" value of the local slopes of the characteristic curve pertaining to the measured pressures. Unfortunately, the method for "weighting" the slopes of the characteristic curves is yet to be established, and so the procedure for obtaining the porosity parameter of a porous wall from its characteristic curve is somewhat unresolved.

It has been shown (ref. 11) that much of the nonlinearity of characteristic curves of perforated walls is eliminated if δ^* is maintained constant for the curve. Thus, for a given wall geometry, one might obtain a different value of R for each value of δ^*. However, during actual model tests, δ^* varies along the walls of the tunnel, being relatively larger at locations of local inflow and much smaller at locations of local outflow. Thus, there still exists the basic problem of finding a method for determining a weighted average of the various R values which represents the gross effect of total boundary. In reference 14, a method is developed whereby the entire upper wall of a two-dimensional tunnel is assumed to be experiencing inflow and the entire lower wall outflow; two separate porosity parameters are employed in the interference corrections, one for each wall. While this method is limited to only two values of R, as opposed to a weighted average of several, it appears superior to the classical method of using a single value of R for the entire tunnel, and is thus a very good step in the right direction.

In the present investigation, the porosity parameters corresponding to 2% outflow have been determined from the curves in figures 19 through 21, and they are presented here for the sake of comparison:

$$R_{2\times2,\ 20.8\%} = 1.1$$

$$R_{11\times11,\ 11.2\%} = 0.41$$

$$R_{11\times11,\ 5.6\%} = 0.14$$

Note, however, that for the two 11- by 11-ft panels, these values of R are only approximately indicative of the porosity parameters of the actual wind-tunnel walls. The reason is that, since crossflow characteristics of porous walls are highly sensitive to boundary-layer displacement thickness,[1] one must take care to match the boundary layer on the wall model to that of the actual tunnel. While the boundary layer of the 2- by 2-ft tunnel has been fairly well duplicated in these model tests, the boundary layer on the 11- by 11-ft model was considerably thinner than in the actual tunnel. Since a thinner boundary layer has the same effect as a decrease in porosity, the values of R for the 11- by 11-ft panels may be somewhat small, that is, the effective porosity of the actual 11- by 11-ft wall is somewhat underestimated.

Two features of the characteristic curves in figures 19 through 21 are immediately apparent. First, there is essentially no effect of change in

[1] See, for example, references 10 and 11.

Mach number on the slopes of the curves. This means that the interference factors[2] for lift and blockage, which are functions of β/R, vary with Mach number for the wall geometries of the present investigation. This is generally the case for all perforated and slotted walls. Secondly, there is only a small effect on the crossflow characteristics of displacing the splitter plate out into the free stream, thereby reducing the boundary layer on the wall models (fig. 19). However, as mentioned above, the boundary layer is known to have an important effect on the crossflow performance of perforated walls. This apparent contradiction can be explained if it is noted that the change in displacement thickness δ^* over the slots because of movement of the splitter plate was much less than the change in δ^* over the slats (see fig. 10). Thus, the effective change in the boundary layer on the wall models because of movement of the panels into the free stream was small; therefore, one would not expect to see a significant change in the crossflow characteristics of the models.

Mean velocity distributions of crossflow measured by a hot wire anemometer just behind the slot of the 2- by 2-ft model are shown in figure 22. The peak crossflow velocity is seen to vary from $\bar{v}$ = 9 m/sec (29.5 ft/sec) at M_∞ = 0.8 to $\bar{v}$ = 22 m/sec (72 ft/sec) at M_∞ = 0.9. The ragged shape of these velocity profiles is attributed to the baffles in the slots.

The root-mean-square values of the fluctuating component of velocity ($\sqrt{\bar{v}'^2}$) parallel to the mean crossflow velocity $\bar{v}$ were also measured by a hot wire for the 2- by 2-ft model. The distribution of the ratio $(\sqrt{\bar{v}'^2})/v$ is shown in figure 23. According to these hot-wire measurements, the fluctuations in crossflow exceeded 30% of the mean crossflow velocity. These values are excessively large compared to those in a turbulent jet or in pipe flow, and further investigation is required in this area. Recent work (ref. 15) has shown that for the Ames 11- by 11-ft wall configuration, organ tones associated with the slot-baffles are responsible for a significant amount of noise in the airstream. Because the 2- by 2-ft wall is similarily baffled, it is conjectured that these fluctuations in crossflow are attributable to organ tones.

Total pressure distributions across the exit of the slots of the wall models were acquired with a traversing probe located in the plenum. From these distributions, an attempt was made to calculate the crossflow velocities, using the difference between the total pressures in the slots and the static pressure in the plenum. However, it was found that, for small crossflow velocities, this difference was generally as small as the instrumentation error of the pressure sensor, ±138 N/m^2 (0.02 psi). Hence, these results are not presented in the present report.

---

[2] See reference 8 for a discussion of interference factors.

CONCLUDING REMARKS

The present investigation was a preliminary step in the study of wall interference on a particular type of transonic wall, that is, a slotted wall with baffle plates in the slots. Two wall models were constructed having the same geometries as the Ames 2- by 2-Foot and 11- by 11-Foot Transonic Wind Tunnels, respectively. The wall models were inserted in the side wall of the Ames 2- by 2-ft tunnel to investigate boundary-layer and crossflow characteristics. The results obtained from this investigation are as follows:

1. For the case of zero mass flow across the walls, a thick boundary layer exists in the region of the slots, with a displacement thickness approximately twice as large as that at the centerline of the solid portion between the slots. When auxiliary suction was applied from behind the walls, the boundary layer over the slots decreased rapidly. With a wall-to-free-stream unit mass flow ratio of $(\rho v)_y/(\rho V)_\infty = 0.02$, the boundary-layer displacement thickness over the slots and over the slats was essentially equal.

2. For the Mach number range from 0.5 to 1.2, δ^* was essentially invariant with Mach number over the slats of the walls for zero mass outflow. Along the slots there was observed an increase in δ^* beginning approximately at $M_\infty = 0.8$, but this increase is attributed to an aspirating effect occurring in the plenum behind the wall models.

3. The effect on the model boundary layers of moving the models into the free stream away from the tunnel wall boundary layer was found to be very small in the vicinity of the slots where the boundary layer was primarily influenced by the disturbances in the slots. As a result and contrary to what was expected, there was only a small change in the crossflow characteristics of the models because of the splitter plate movement.

4. The static pressure along the tunnel centerline was very uniform for both wall models. Deviations from the mean pressure were of the order of 0.1% at lateral distances of 20 and 26 slot widths for the 11- by 11-ft and the 2- by 2-ft models, respectively.

5. Crossflow characteristic curves of the wall models resulted in porosity parameters of $R = 1.1$ for the 2- by 2-ft model (20.8% porosity) and $R = 0.14$ for the 11- by 11-ft model (5.6% porosity). The porosity parameters were independent of free-stream Mach number. Consequently, the interference factors, which depend on β/R, vary with M_∞ for the wall configurations tested.

6. Peak crossflow velocities increased from $V_{max} = 9$ m/sec at $M_\infty = 0.8$ to $V_{max} = 22$ m/sec at $M_\infty = 0.9$, even though the ratio of wall-to-free-stream mass flow per unit area decreased at a fixed auxiliary pump speed. Hot-wire measurements indicate very high fluctuations in crossflow velocity parallel to the mean crossflow velocity.

As a result of the present study, it has been determined that further investigations should be made to get a more complete understanding of the

boundary conditions near the type of slotted wall described herein. In particular, it would be desirable to perform a similar experiment using traversing rather than fixed boundary-layer probes, measuring the boundary-layer growth along the slots and slats and the variation in boundary layer transverse to the flow. The development of hot-wire anemometry for crossflow measurements is desirable in order to get more detailed information on the turbulent flows across the walls and their effect on the wall crossflow characteristics. The crossflow velocity should be measured at several streamwise stations along the slots, especially near the downstream end, to determine the distribution of flow removal. Detailed surveys of pressure and flow angles near the walls should also be conducted to determine the extent of three-dimensional flow patterns near the slots.

Finally, to derive more beneficial information from characteristic curves of porous walls, a method needs to be developed for choosing an "average" porosity parameter that accounts for both inflow and outflow through tunnel walls during model testing. Such a method may well involve measurement of the conditions at the tunnel walls during actual model tests.

Ames Research Center
National Aeronautics and Space Administration
Moffett Field, California 94035, June 24, 1977

REFERENCES

1. Davis, Don D., Jr.; and Moore, Dewey: Analytical Study of Blockage- and Lift-Interference Corrections for Slotted Tunnels Obtained by the Substitution of an Equivalent Homogeneous Boundary for the Discrete Slots. NACA RM L53E07b, 1953.

2. Maeder, Paul F.: Theoretical Investigation of Subsonic Wall Interference in Rectangular Slotted Test Sections. Tech. Rep. WT-11, 1953.

3. Guderley, K. Gottfried: Wall Corrections for a Wind Tunnel With Longitudinal Slots at Subsonic Velocities. WADC TR 54-22, 1954.

4. Goethert, B. H.: Properties of Test Section Walls With Longitudinal Slots in Curbed Flow for Subsonic and Supersonic Velocities (Theoretical Investigations). AEDC-TN-55-56, 1957.

5. Chen, C. F.; and Mears, J. W.: Experimental and Theoretical Study of Mean Boundary Conditions of Perforated and Longitudinally Slotted Wind Tunnel Walls. AEDC-TR-58-20, 1957.

6. Ebihara, Masao: A Study of Subsonic, Two-Dimensional Wall-Interference Effect in a Perforated Wind Tunnel With Particular Reference to the NAL 2 M by 2 M Transonic Wind Tunnel: Inapplicability of the Conventional Boundary Condition. NAL-TR-252T, 1972.

7. Wood, W. W.: Tunnel Interference From Slotted Walls. Quart. Jour. Mech. and Appl. Math, vol. 17, pt. 2, 1964, pp. 125-140.

8. Pindzola, M.; and Lo, C. F.: Boundary Interference at Subsonic Speeds in Wind Tunnels With Ventilated Walls. AEDC-TR-69-47, 1969.

9. Chew, William L.: Crossflow Calibration at Transonic Speeds of Fourteen Perforated Plates With Round Holes and Airflow Parallel to the Plates. AEDC-TR-54-65, 1955.

10. Goethert, Bernhard H.: Transonic Wind Tunnel Testing. AGARDograph 49, Pergamon Press, 1961.

11. Lukasiewicz, J.: Effects of Boundary Layer and Geometry on Characteristics of Perforated Wall for Transonic Wind Tunnels. Aerosp. Eng., vol. 20, no. 4, 1961, pp. 22-23, 62-68.

12. Muhlstein, Lado, Jr.; Gaspers, Peter A., Jr.; and Riddle, Dennis W.: An Experimental Study of the Influence of the Turbulent Boundary Layer on Panel Flutter. NASA TN D-4486, 1968.

13. Fluid Meters; Their Theory and Application. Report of the ASME Research Committee on Fluid Meters, Fifth Edition, 1959.

14. Mokry, M.; Peake, P. J.; and Bowker, A. J.: Wall Interference on Two-Dimensional Supercritical Airfoils, Using Wall Pressure Measurements to Determine the Porosity Factors for Tunnel Floor and Ceiling. National Aeronautical Establishment, Canada. Aeronautical Rep. LR-575, 1974.

15. Dougherty, N. S., Jr.; and Steinle, F. W., Jr.: Transition Reynolds Number Comparisons in Several Major Transonic Tunnels. AIAA Paper No. 74-627, July 1974.

Note: All dimensions are
in meters (inches)

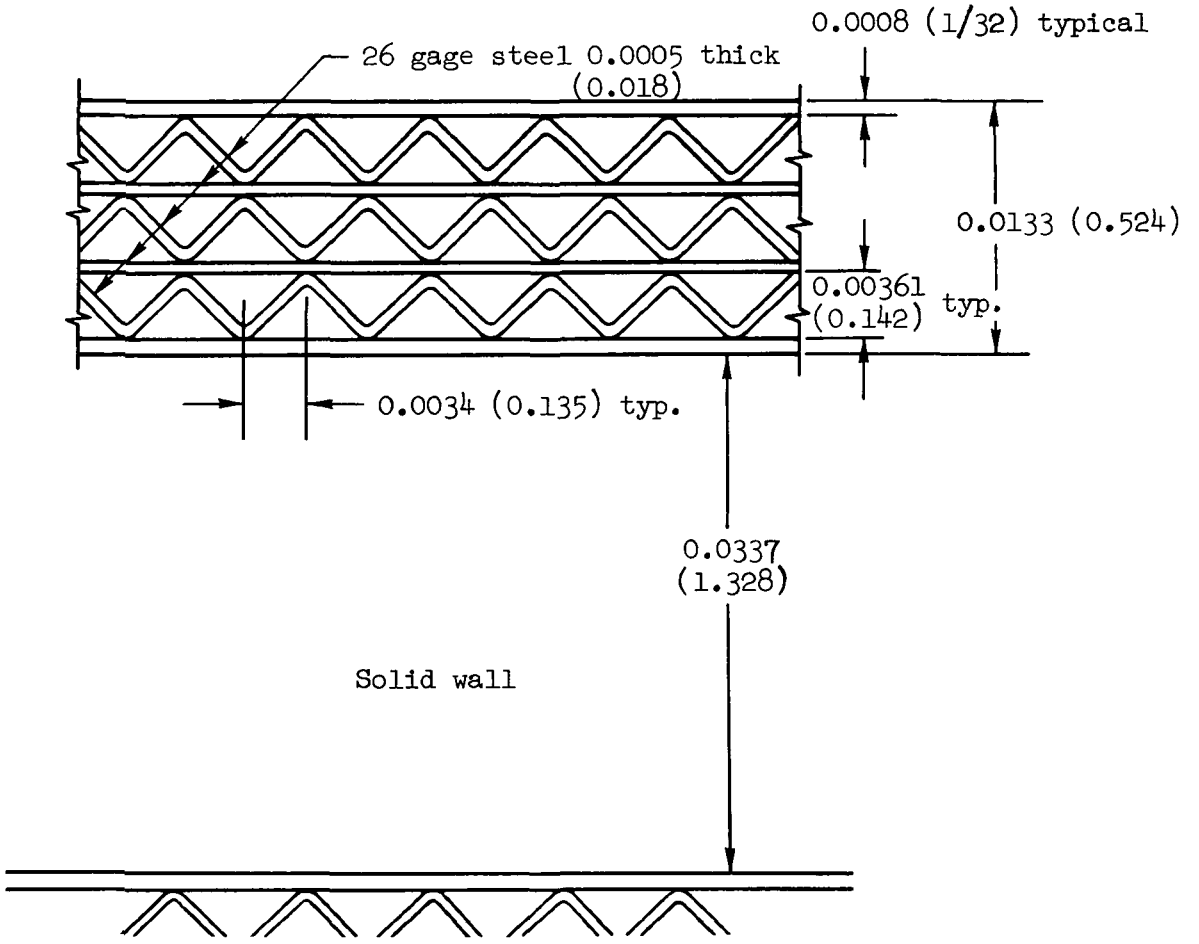

Figure 1.- Slotted walls of the Ames 2- by 2-Foot Transonic Wind Tunnel, with baffle-plate inserts.

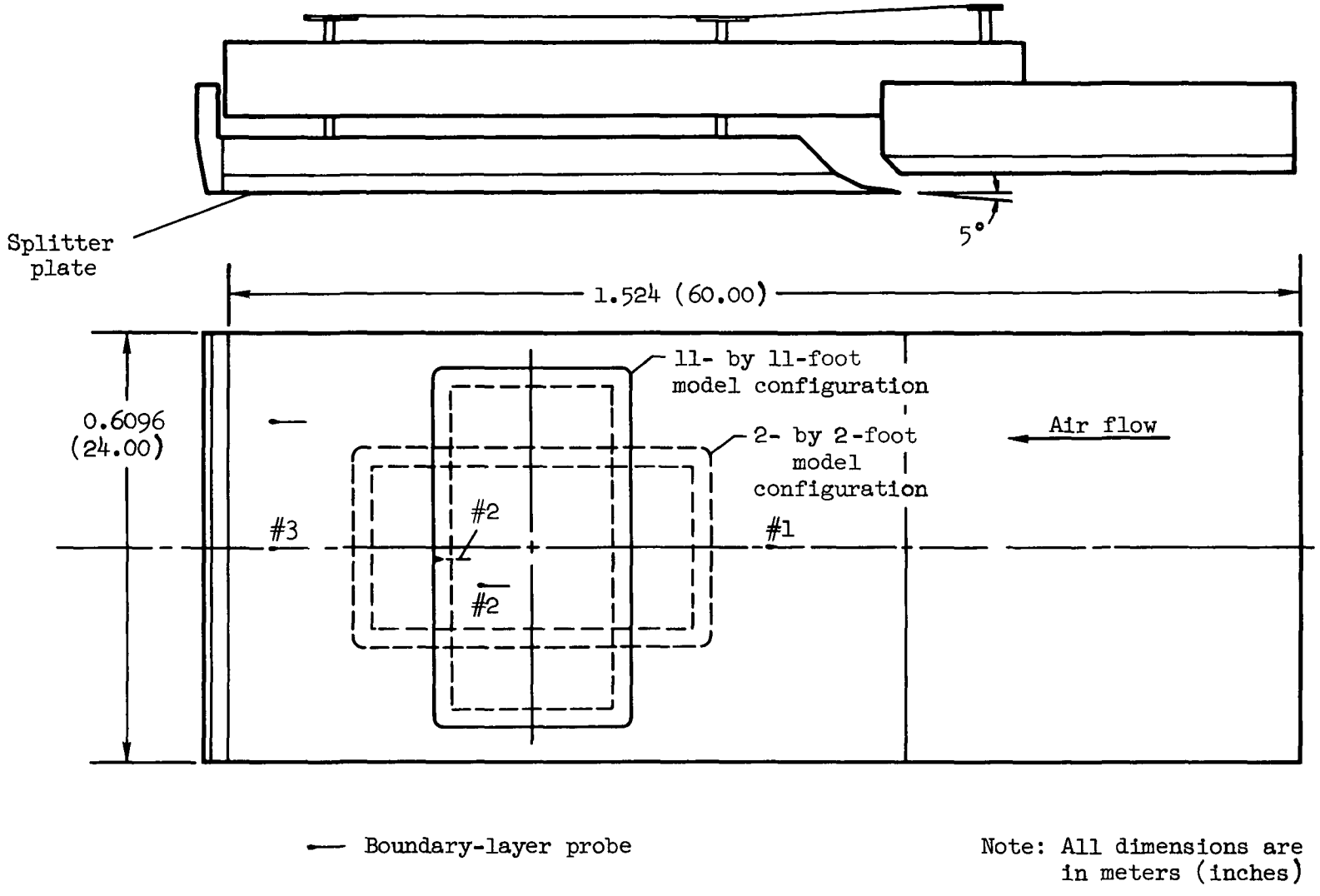

Figure 2.- Layout of variable boundary-layer wall frame showing two wall model configurations.

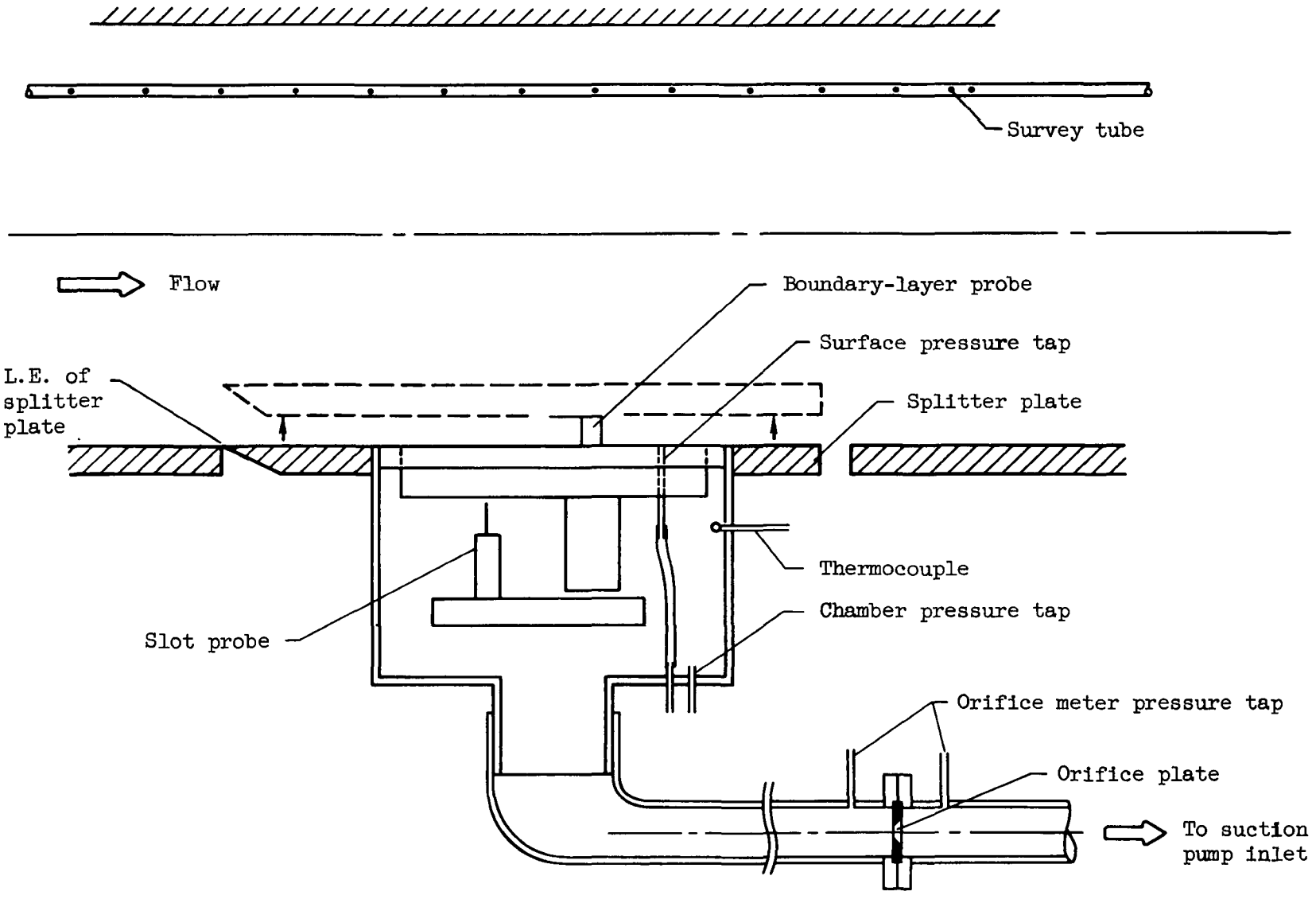

Figure 3.- Schematic view of the test apparatus.

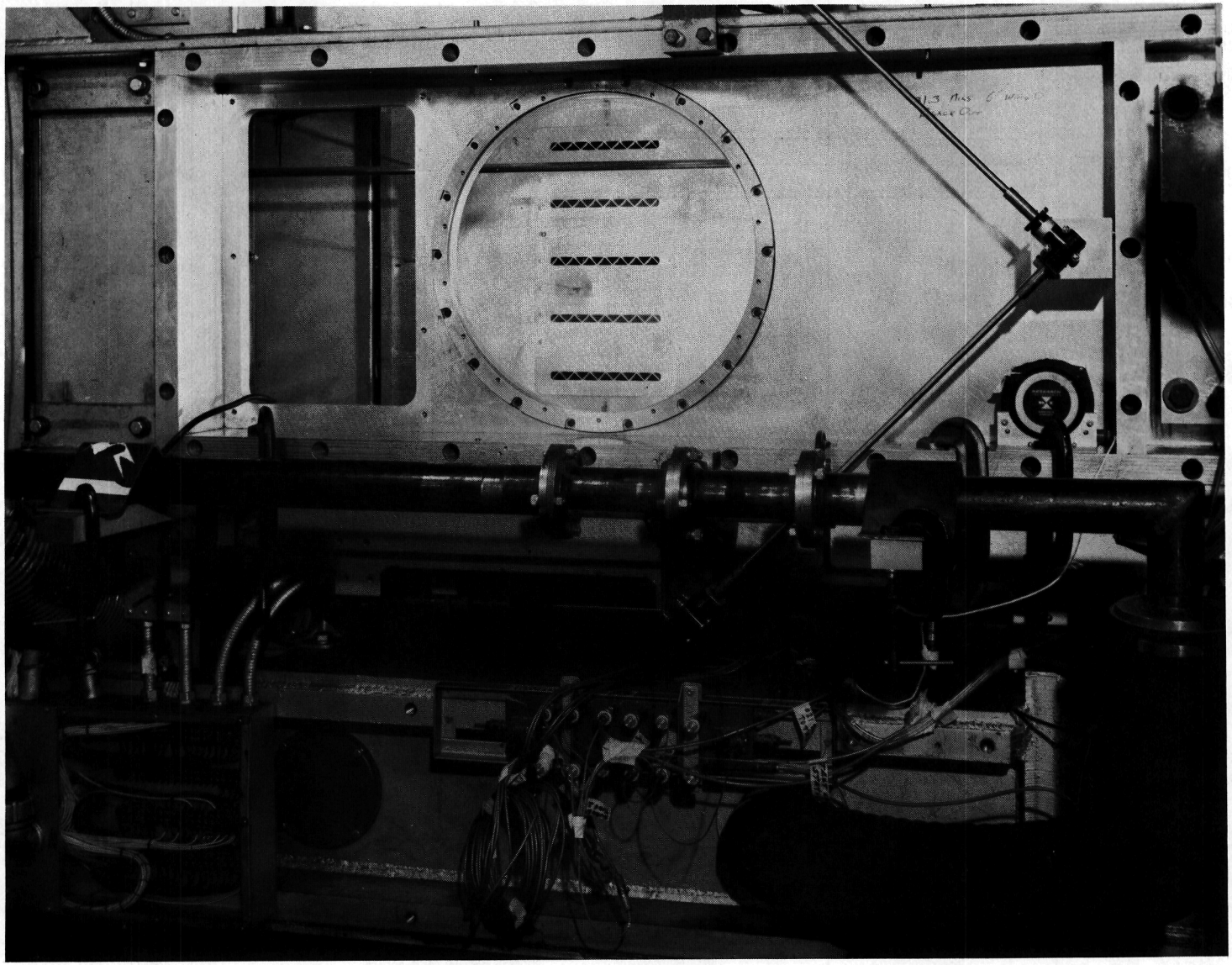

Figure 4.- Test section of 2- by 2-ft transonic wind tunnel with 11- by 11-ft wall panel mounted inside wall (flow right to left).

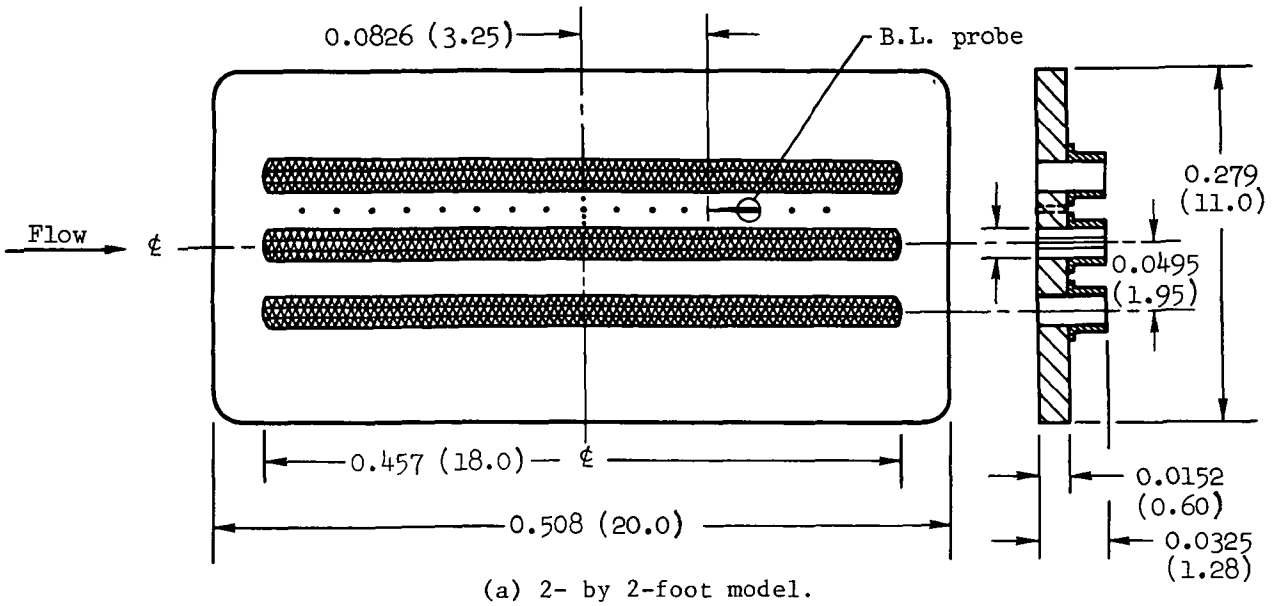

(a) 2- by 2-foot model.

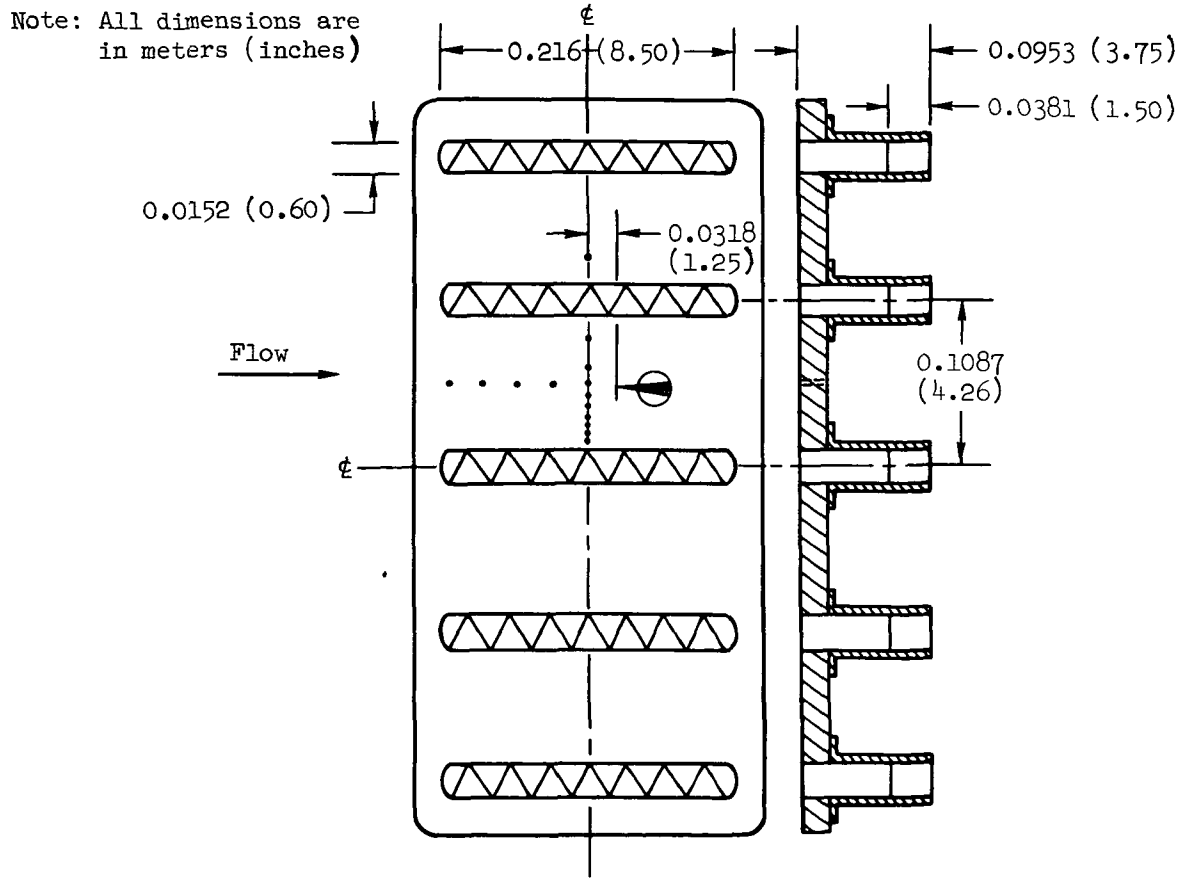

(b) 11- by 11-foot model.

Figure 5.- Sketches of the two wall models.

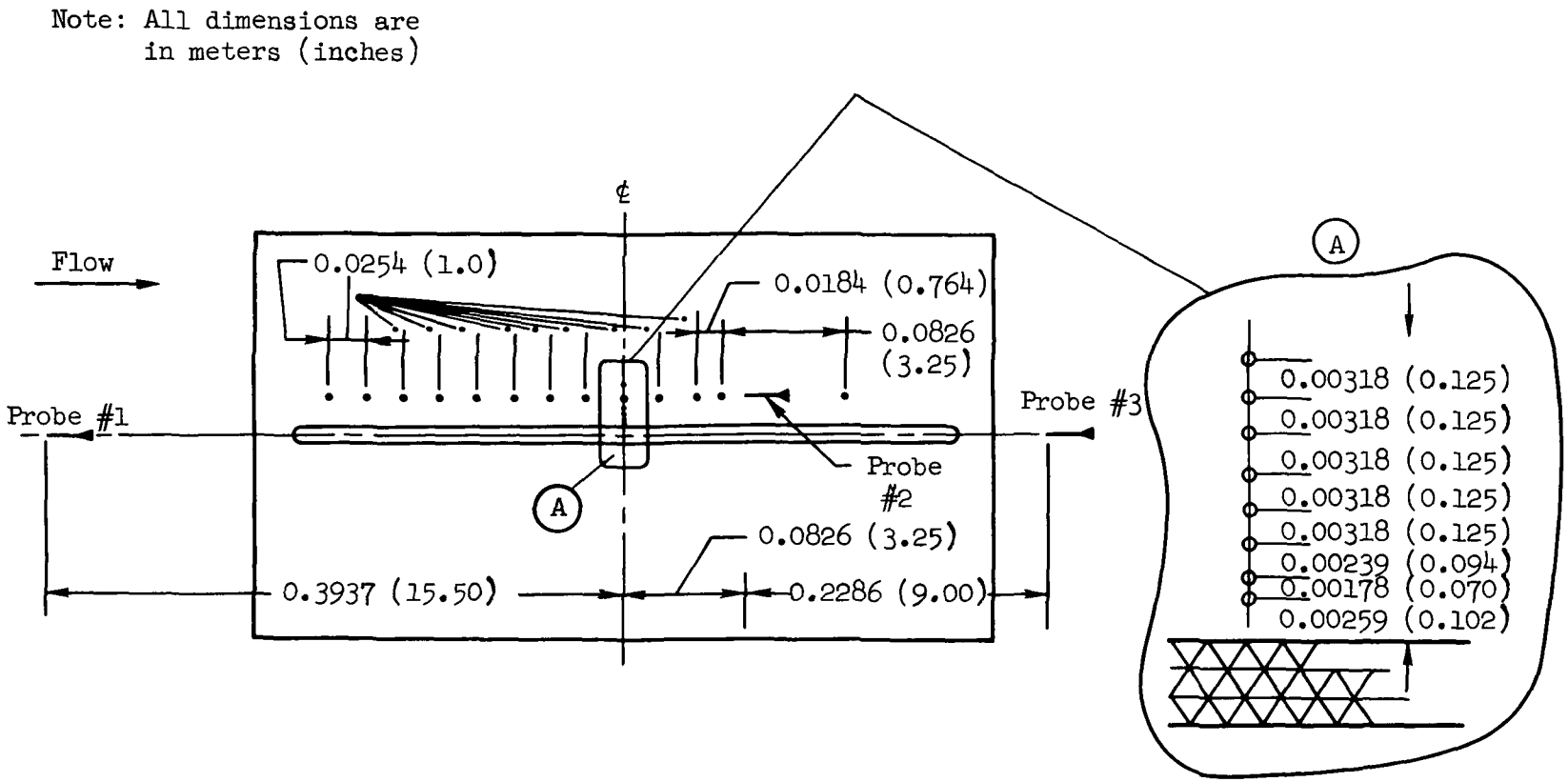

(a) 2- by 2-ft model.

Figure 6.- Locations of surface pressure taps and boundary-layer probes.

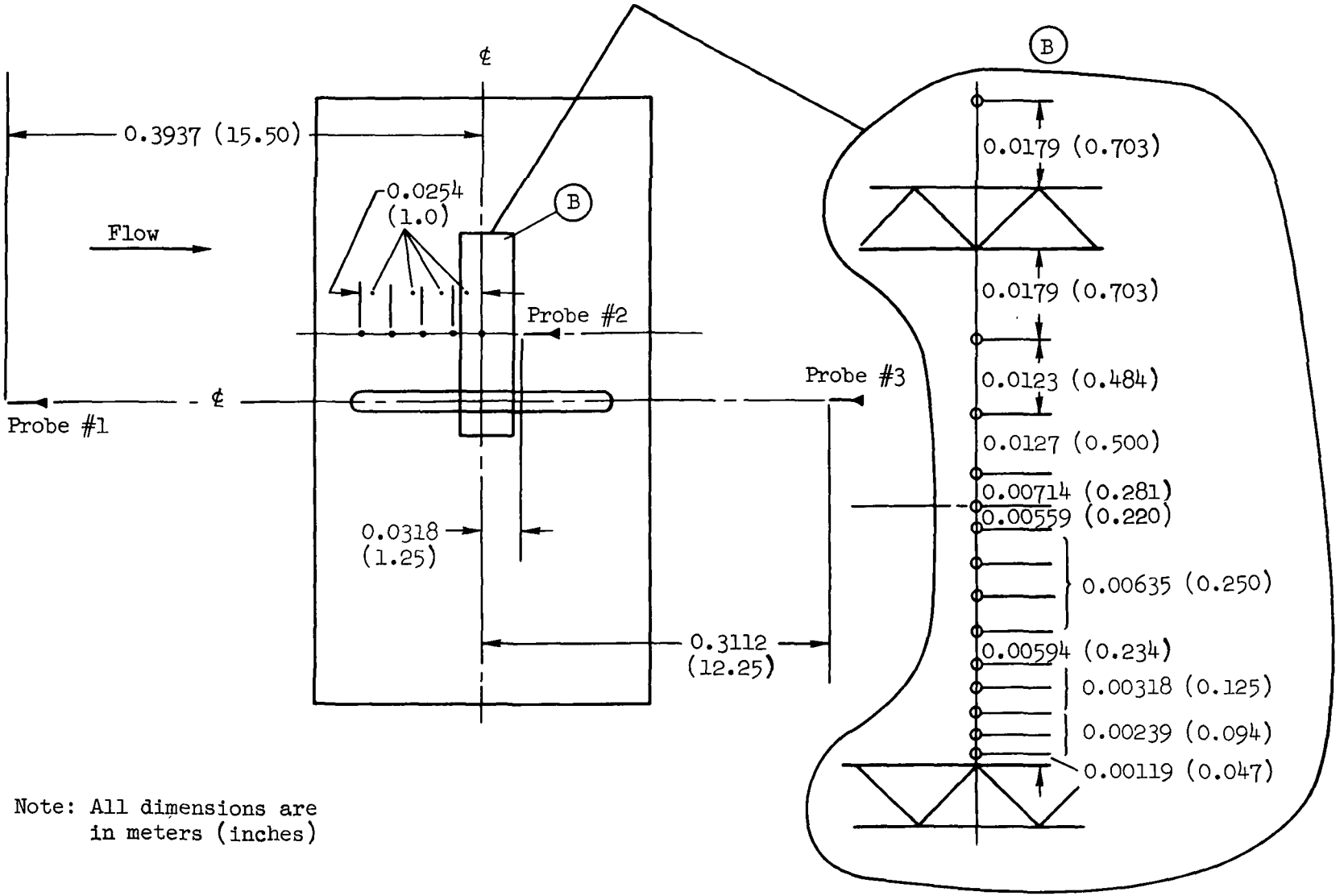

Note: All dimensions are in meters (inches)

(b) 11- by 11-ft model.

Figure 6.- Concluded.

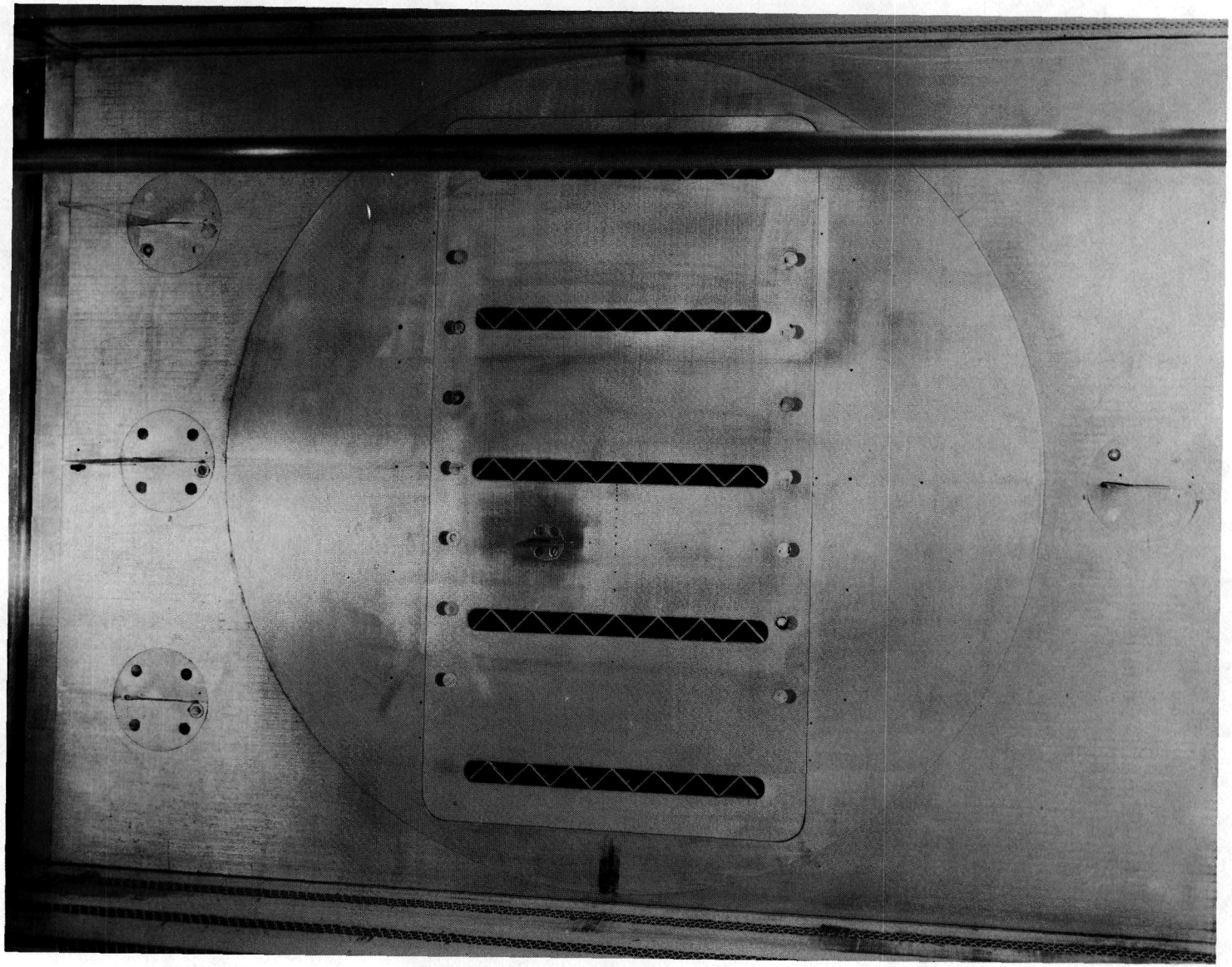

Figure 7.- Model of the 11- by 11-ft wall showing surface pressure survey taps, boundary-layer probes and static-pressure survey tube (flow right to left).

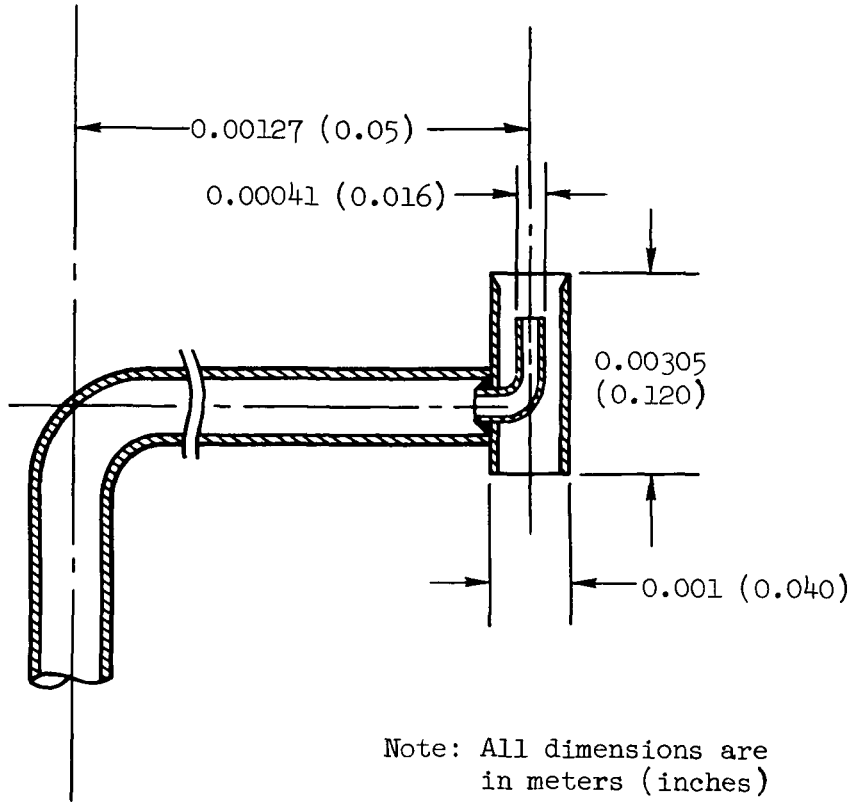

Figure 8.- Total pressure probe tip for pressure measurement behind the slot.

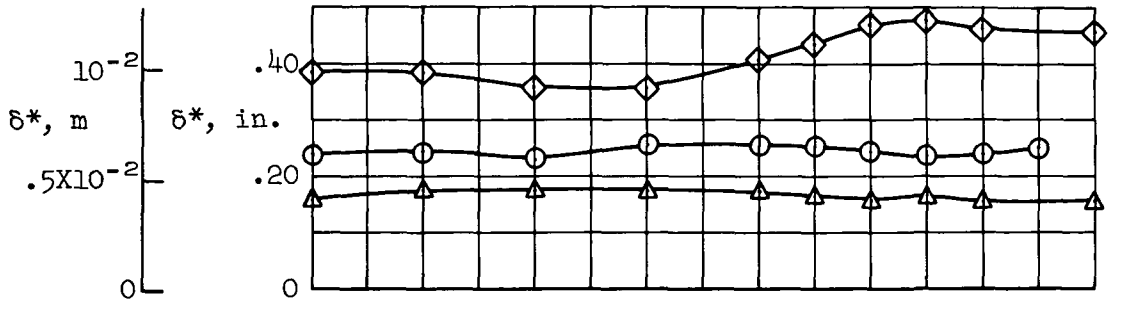

(a) 2- by 2-foot panel - 20.8% open.

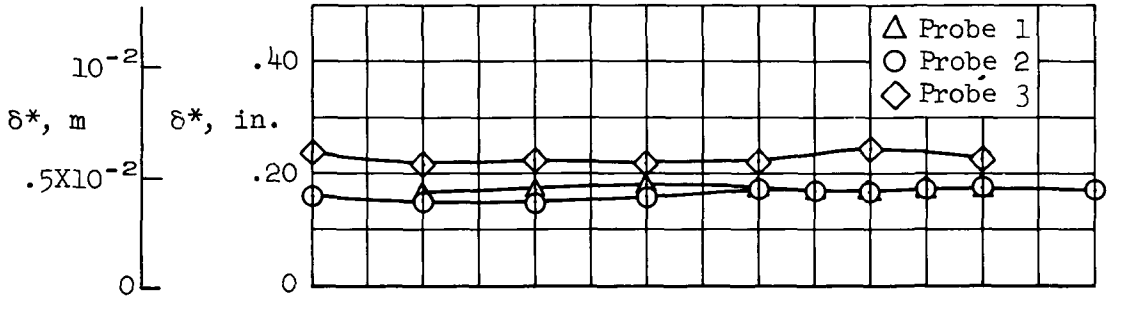

(b) 11- by 11-foot panel - 11.2% open.

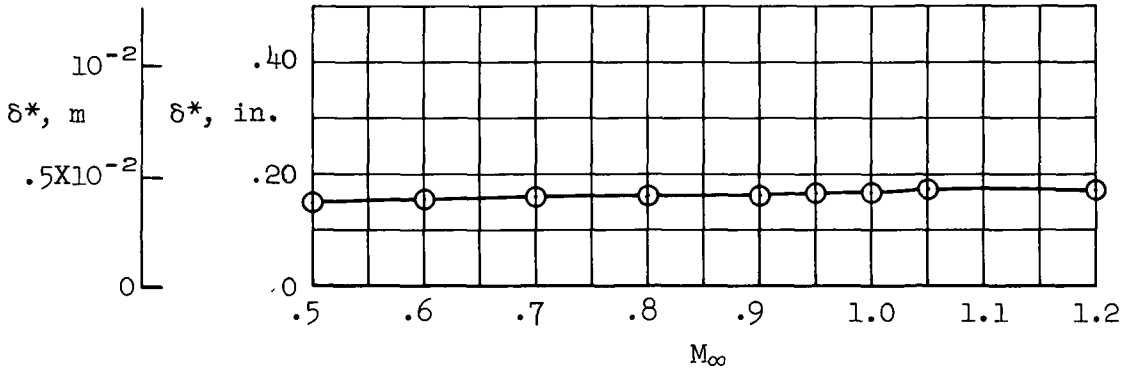

(c) 11- by 11-foot panel - 5.6% open.

Figure 9.- Boundary-layer displacement thickness vs free-stream Mach number (no auxiliary suction).

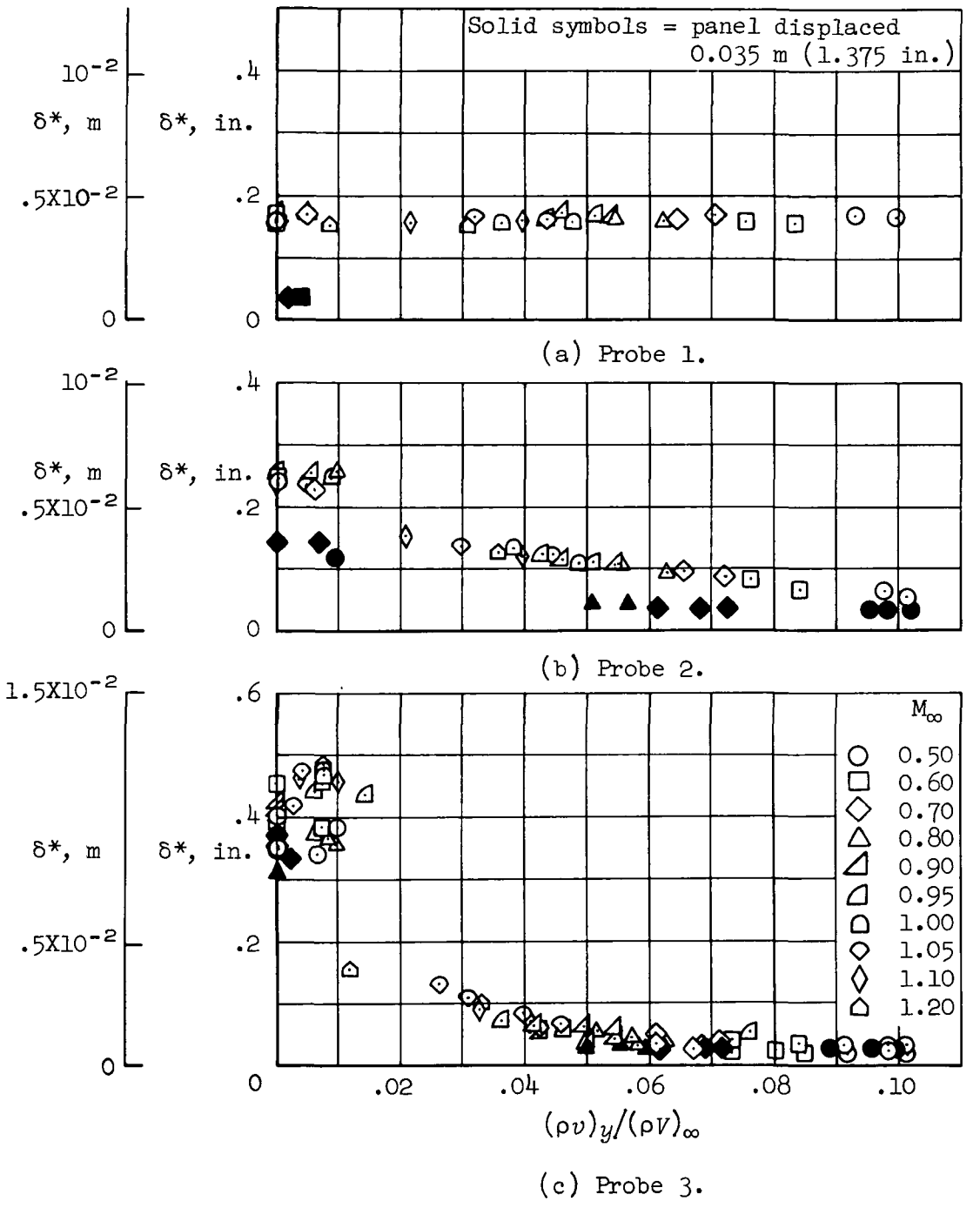

Figure 10.- Boundary-layer displacement thickness vs mass outflow ratio for 2- by 2-ft panel.

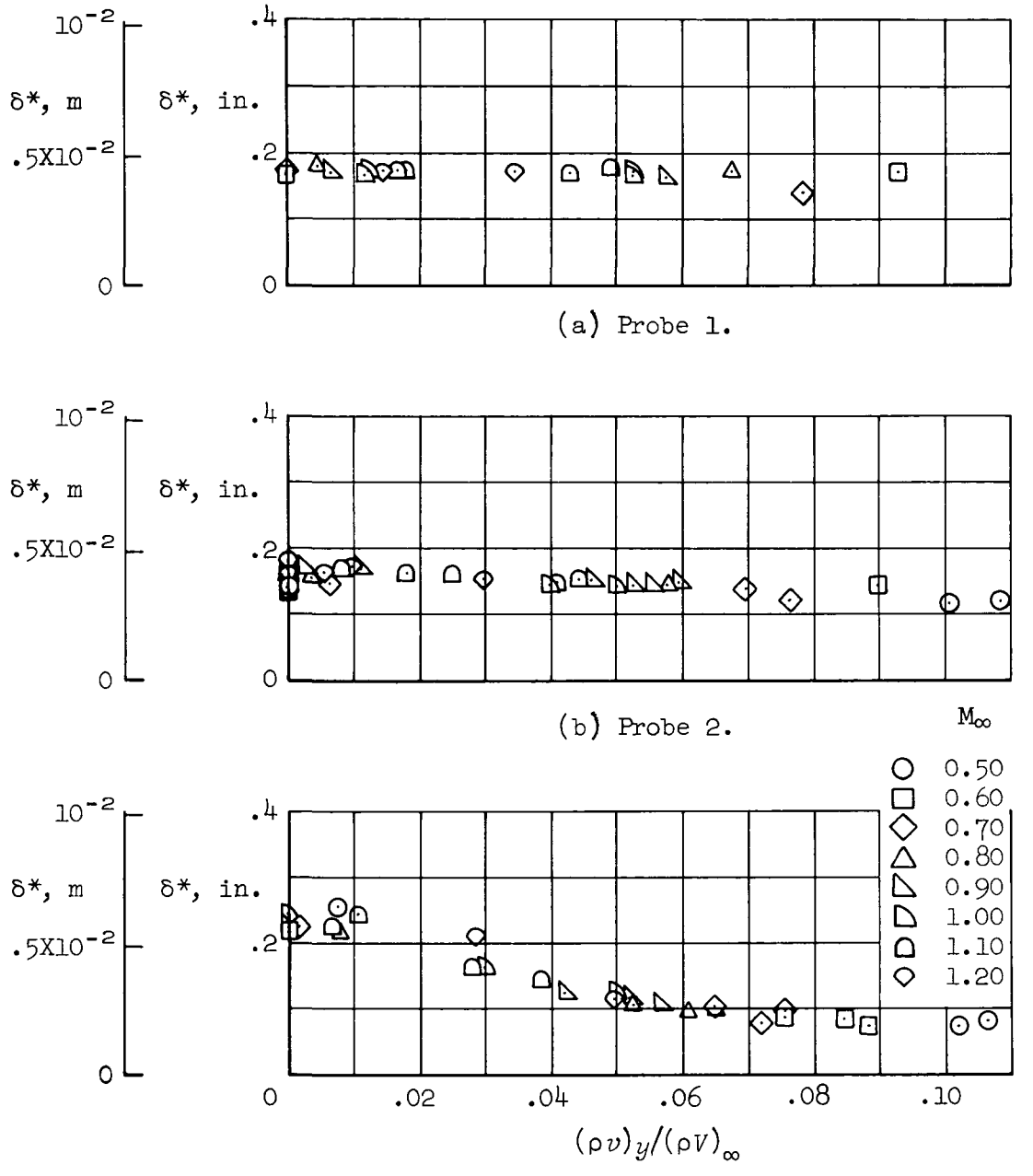

Figure 11.- Boundary-layer displacement thickness vs mass outflow ratio for 11- by 11-ft panel (11.2% open).

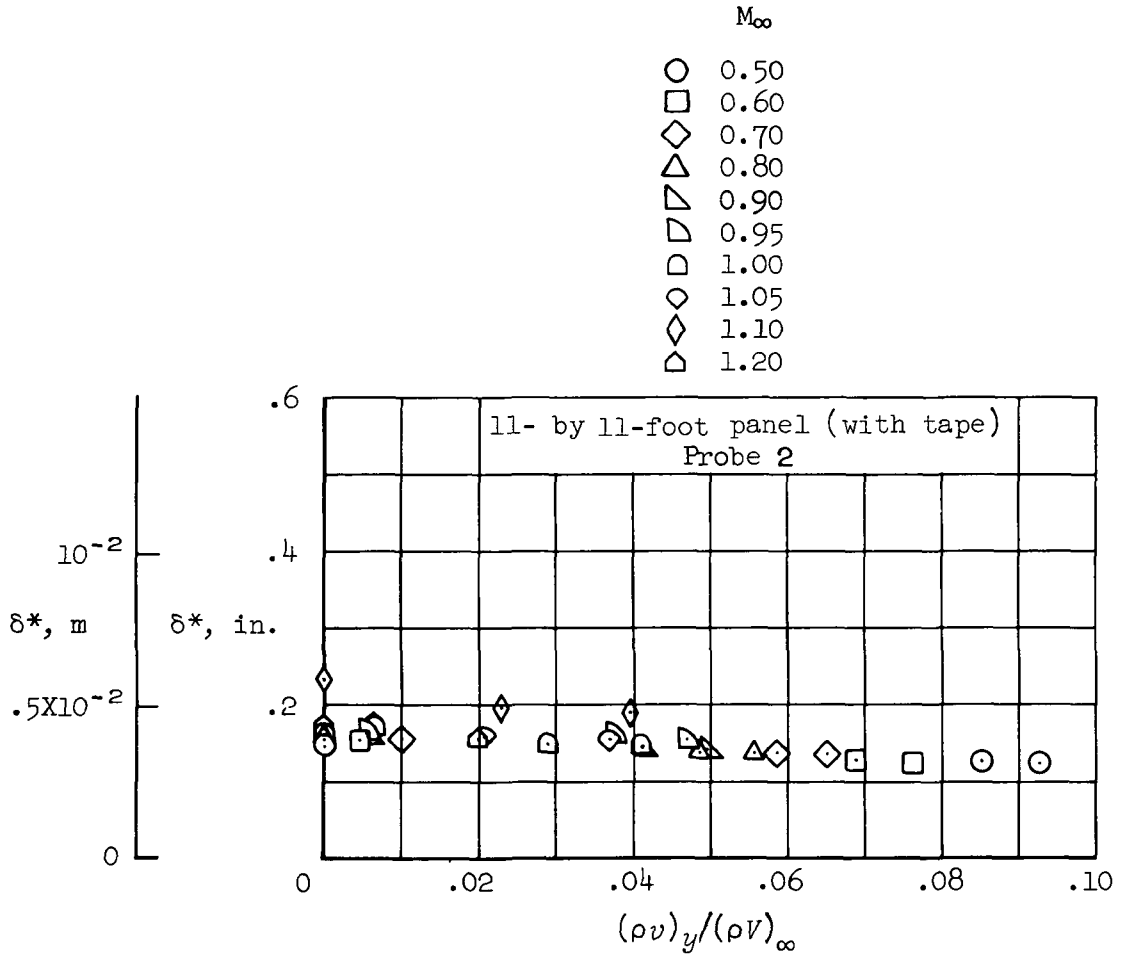

Figure 12.- Boundary-layer displacement thickness vs mass outflow ratio for 11- by 11-ft panel (5.6% open).

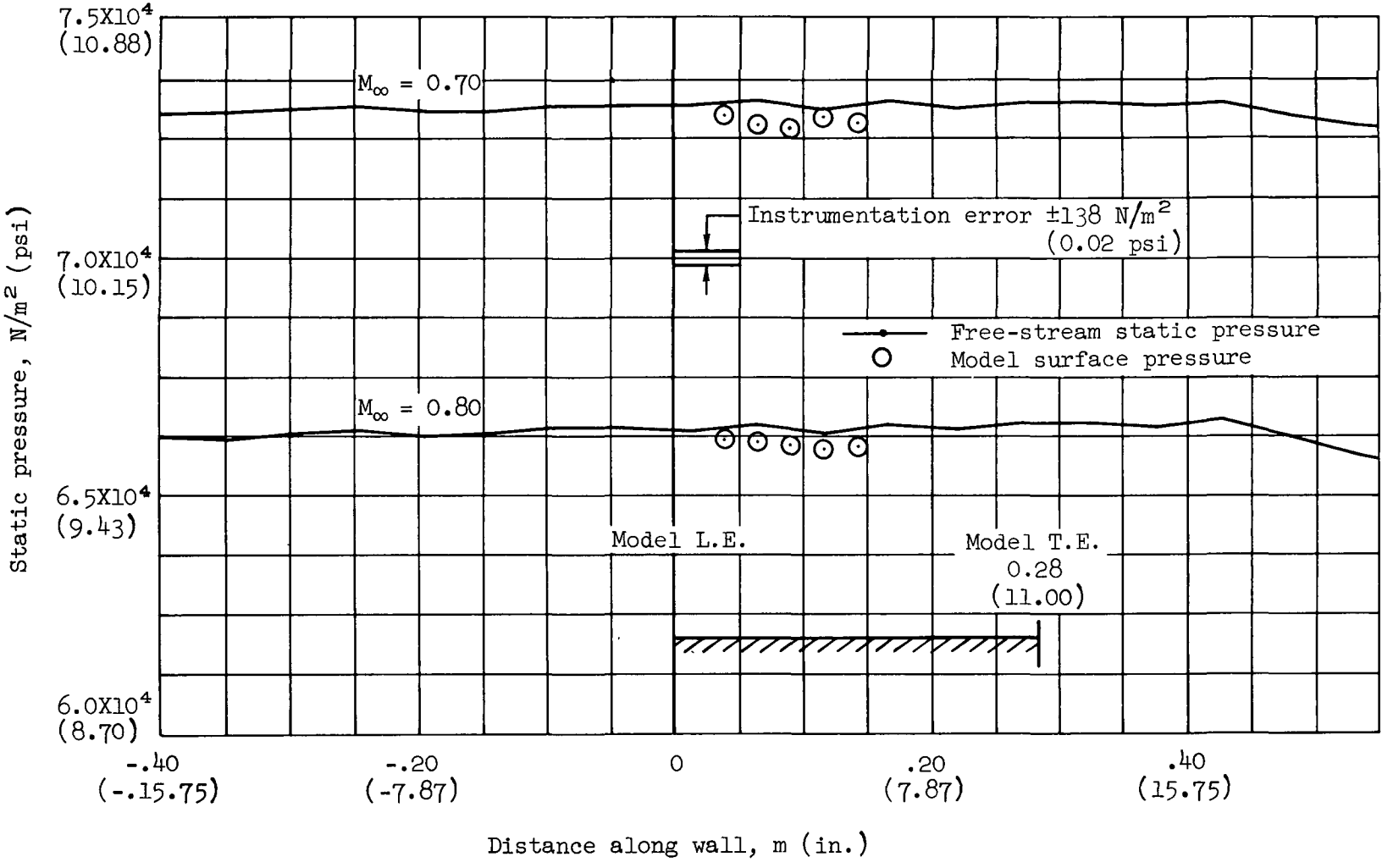

Figure 13.- Free-stream static pressures and surface pressures on the 11- by 11-ft model along streamwise direction; $(\rho v)_y/(\rho V)_\infty = 0.003$.

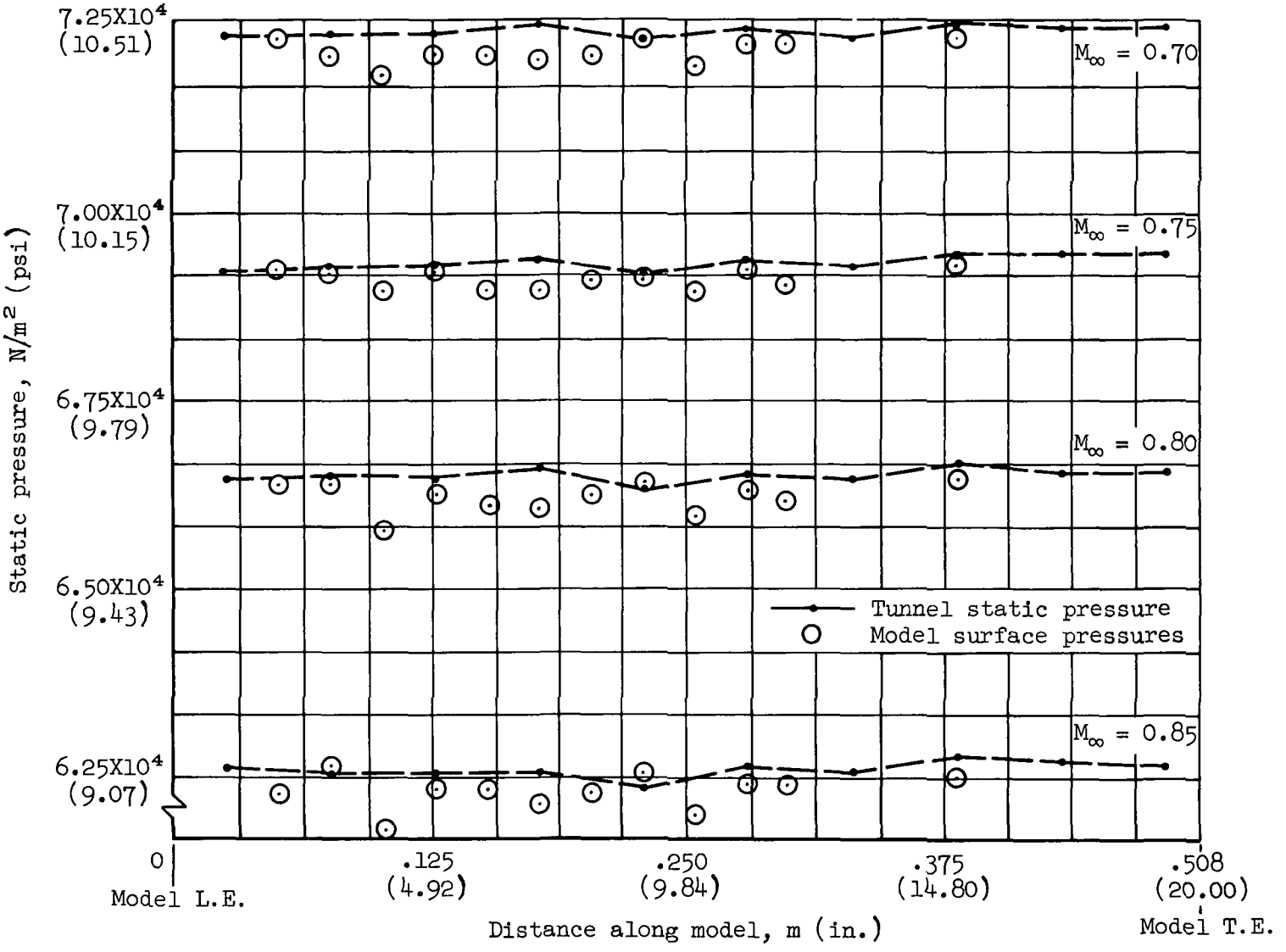

Figure 14.- Static pressures in the tunnel and surface pressures on the 2- by 2-ft model along streamwise direction; $(\rho v)_y/(\rho V)_\infty = 0.004$.

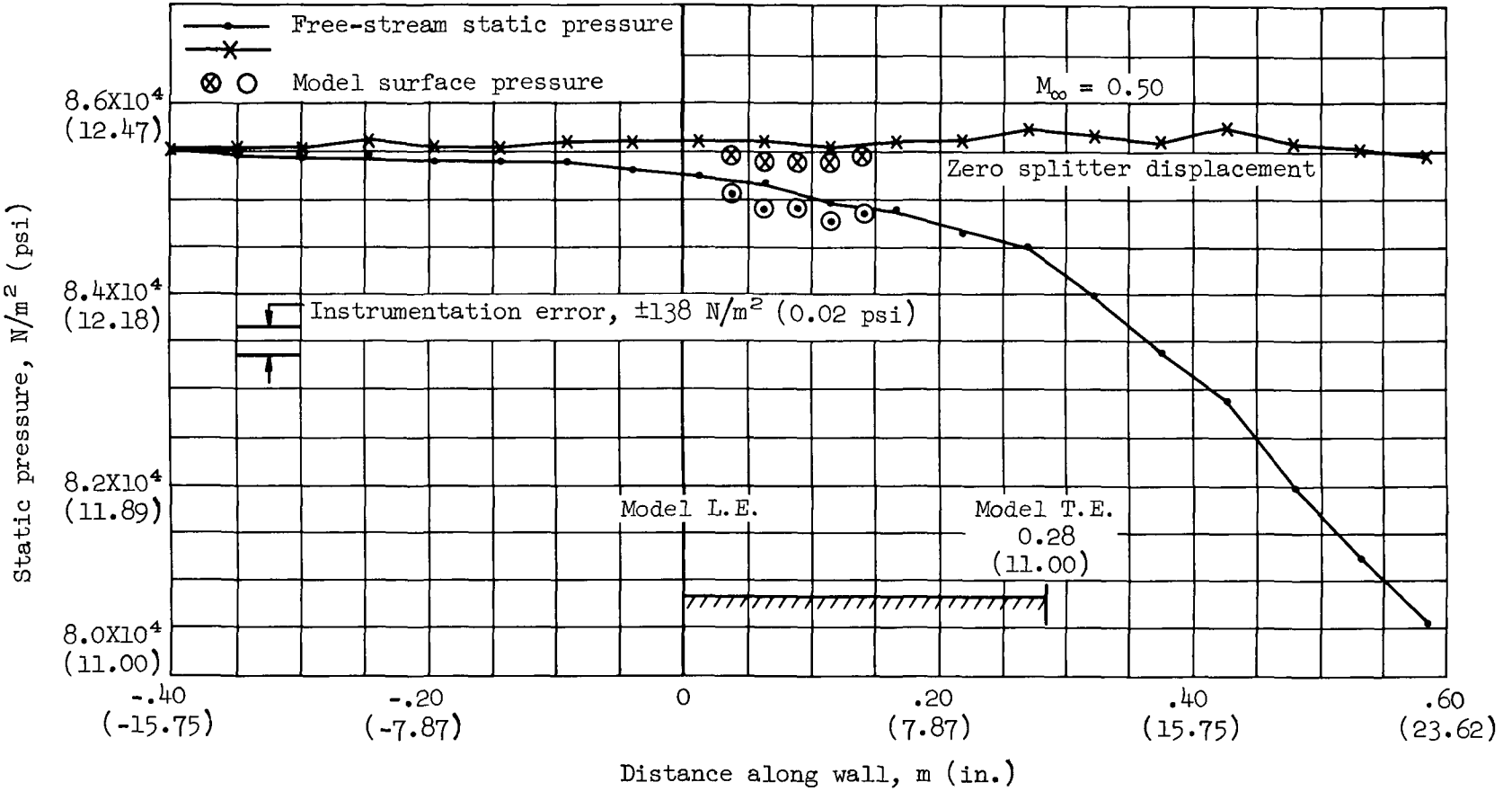

Figure 15.- Free-stream static pressures and surface pressures on the 11- by 11-ft model along free-stream direction with and without splitter plate displacement of 0.051 m (2.00 in.).

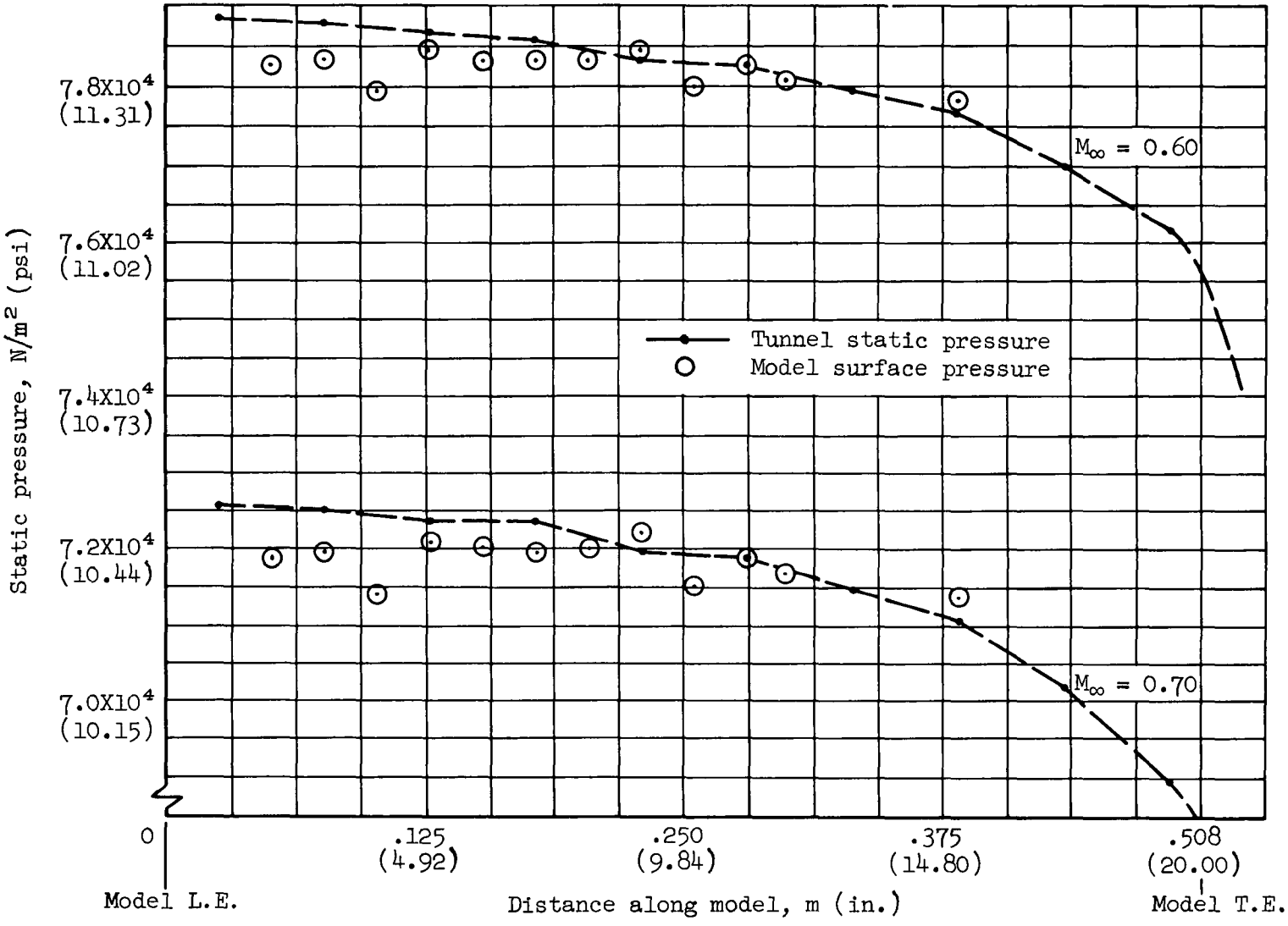

Figure 16.- Free-stream static pressures and surface pressures on the 2- by 2-ft model along free-stream direction with splitter plate moved 0.051 m (2.00 in.) into stream.

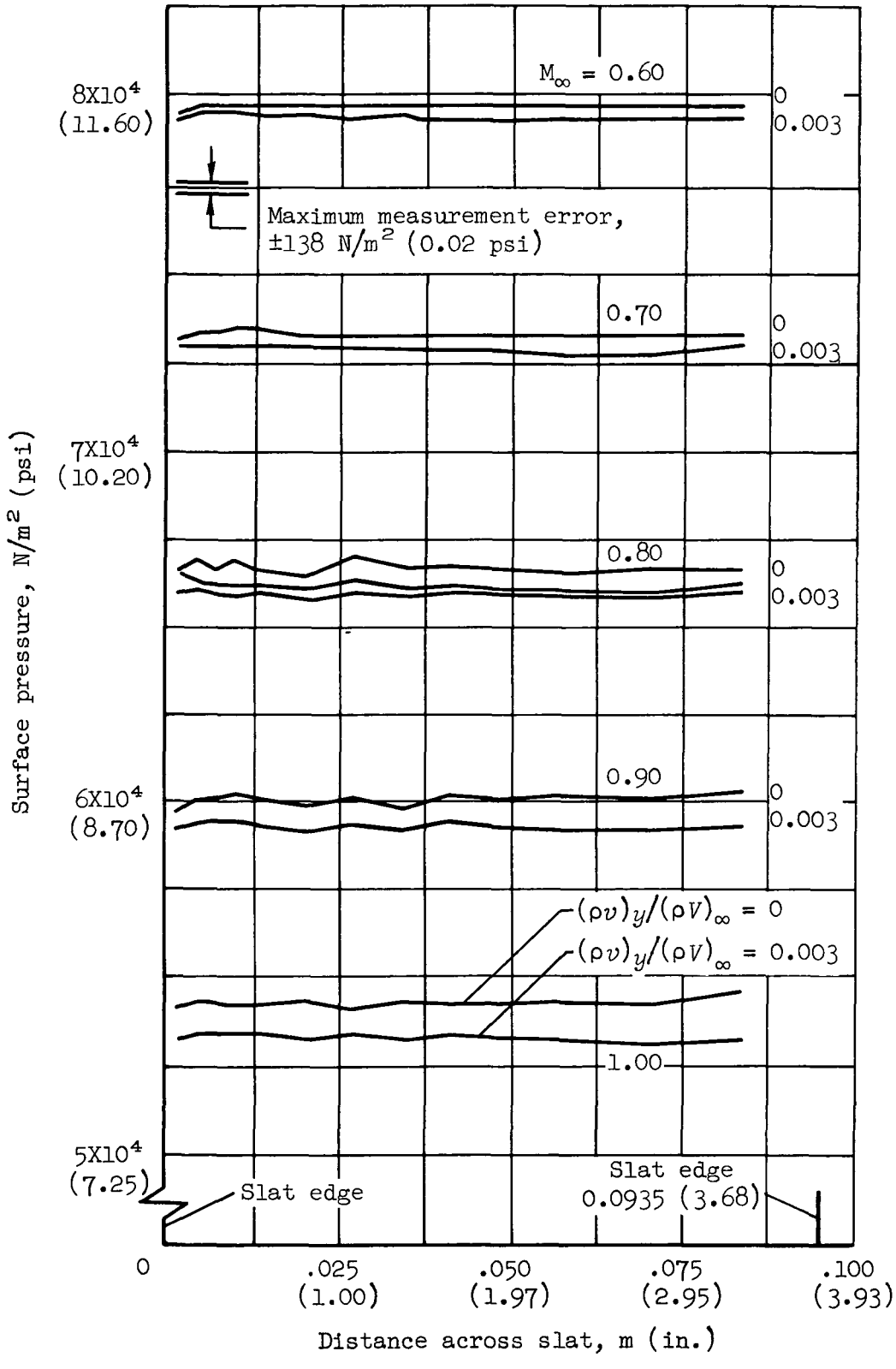

Figure 17.- Surface pressures on the 11- by 11-ft model transverse to free-stream direction.

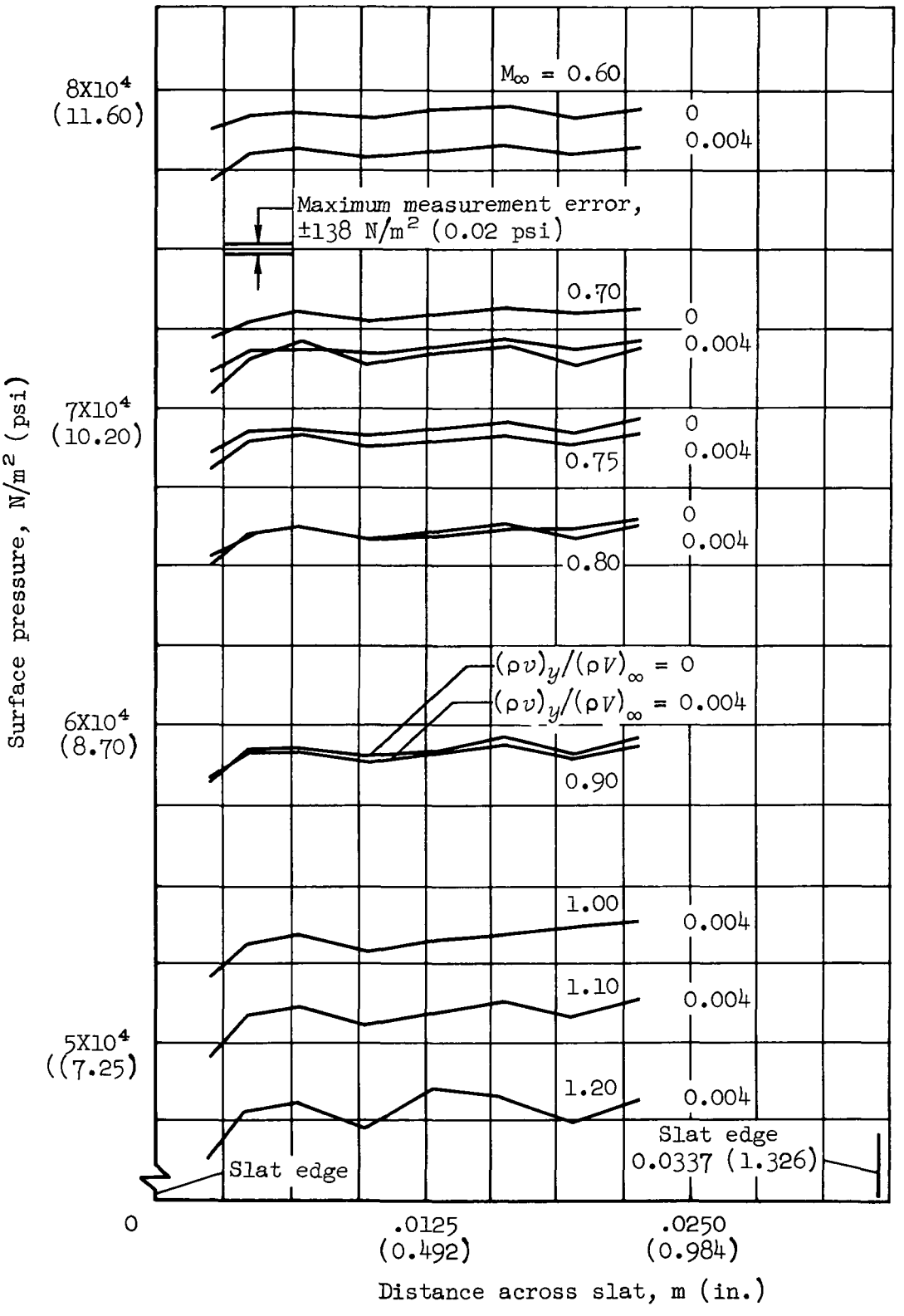

Figure 18.- Surface pressures on the 2- by 2-ft model transverse to free-stream direction.

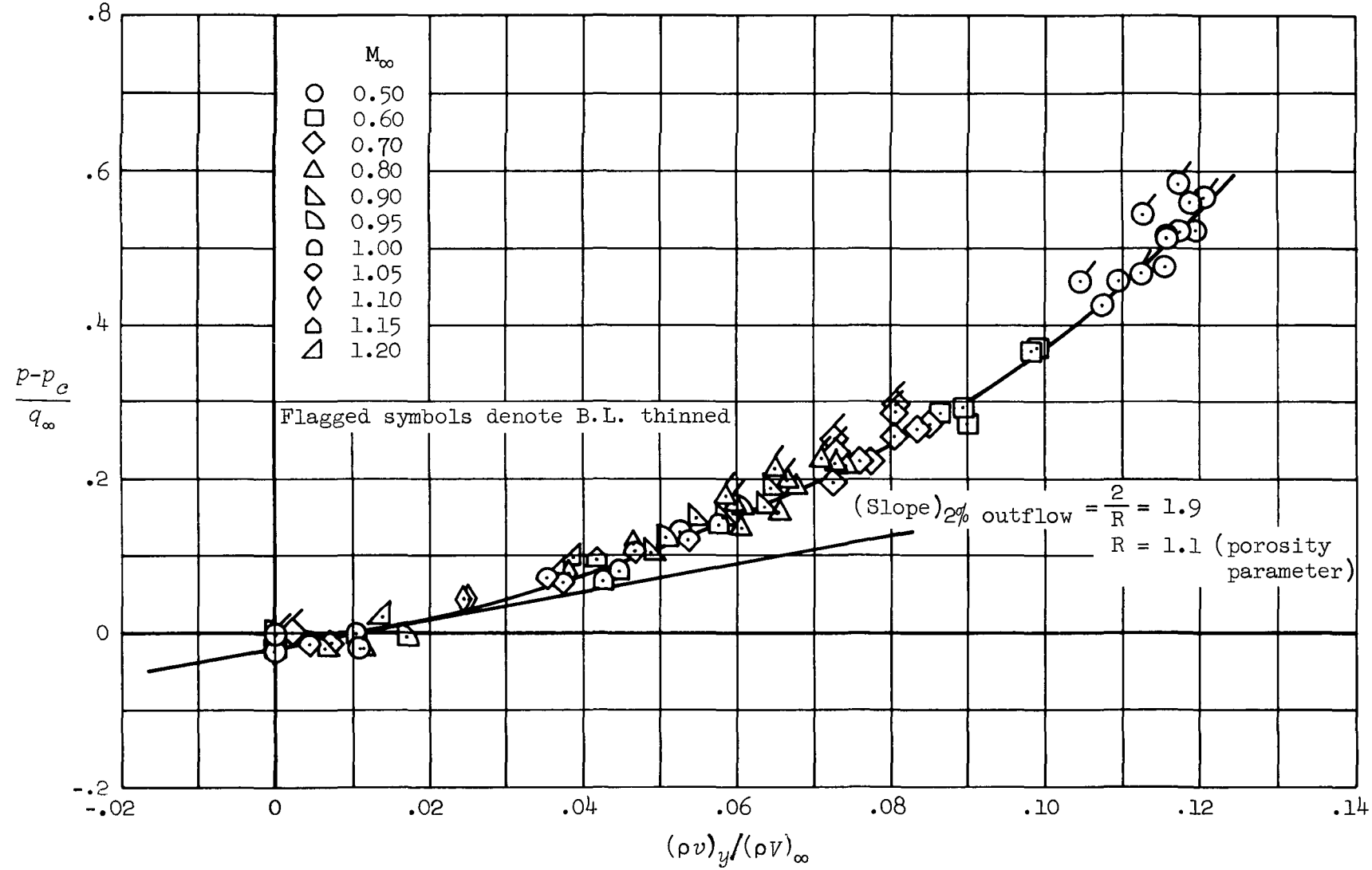

Figure 19.- Crossflow characteristics of 2- by 2-ft panel (20.8% open).

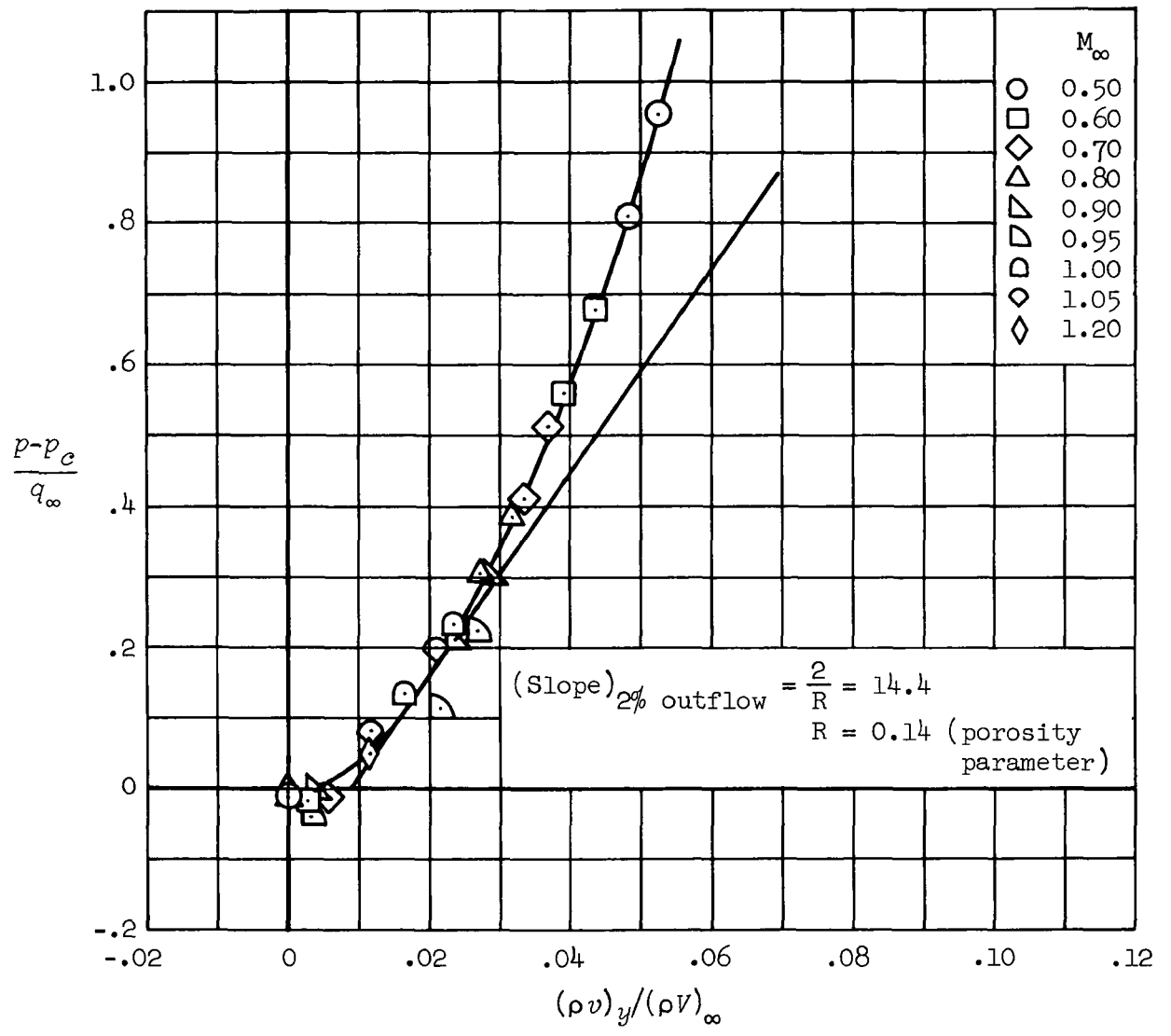

Figure 20.- Crossflow characteristics of 11- by 11-ft panel (5.6% open).

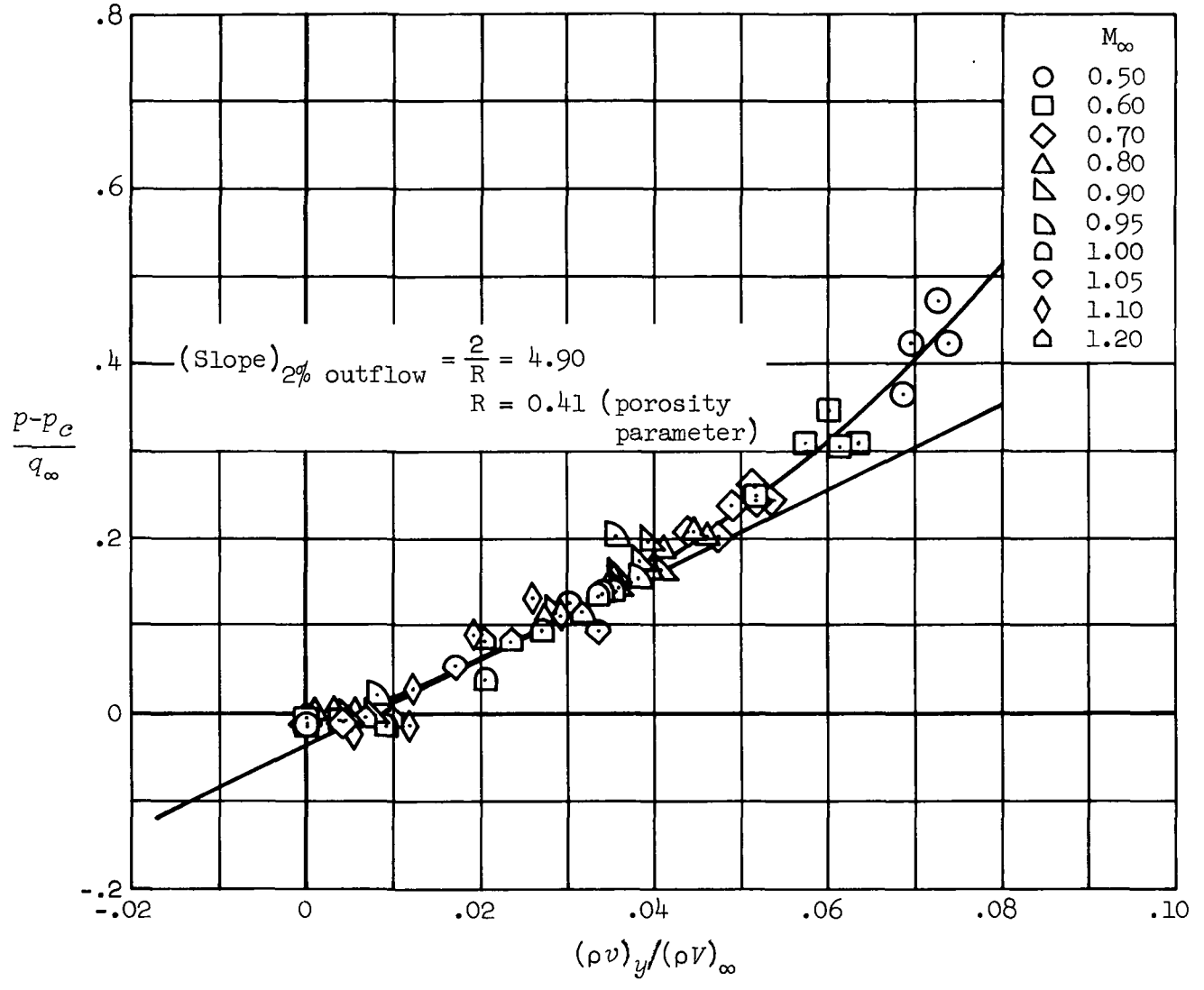

Figure 21.- Crossflow characteristics of 11- by 11-ft panel (11.2% open).

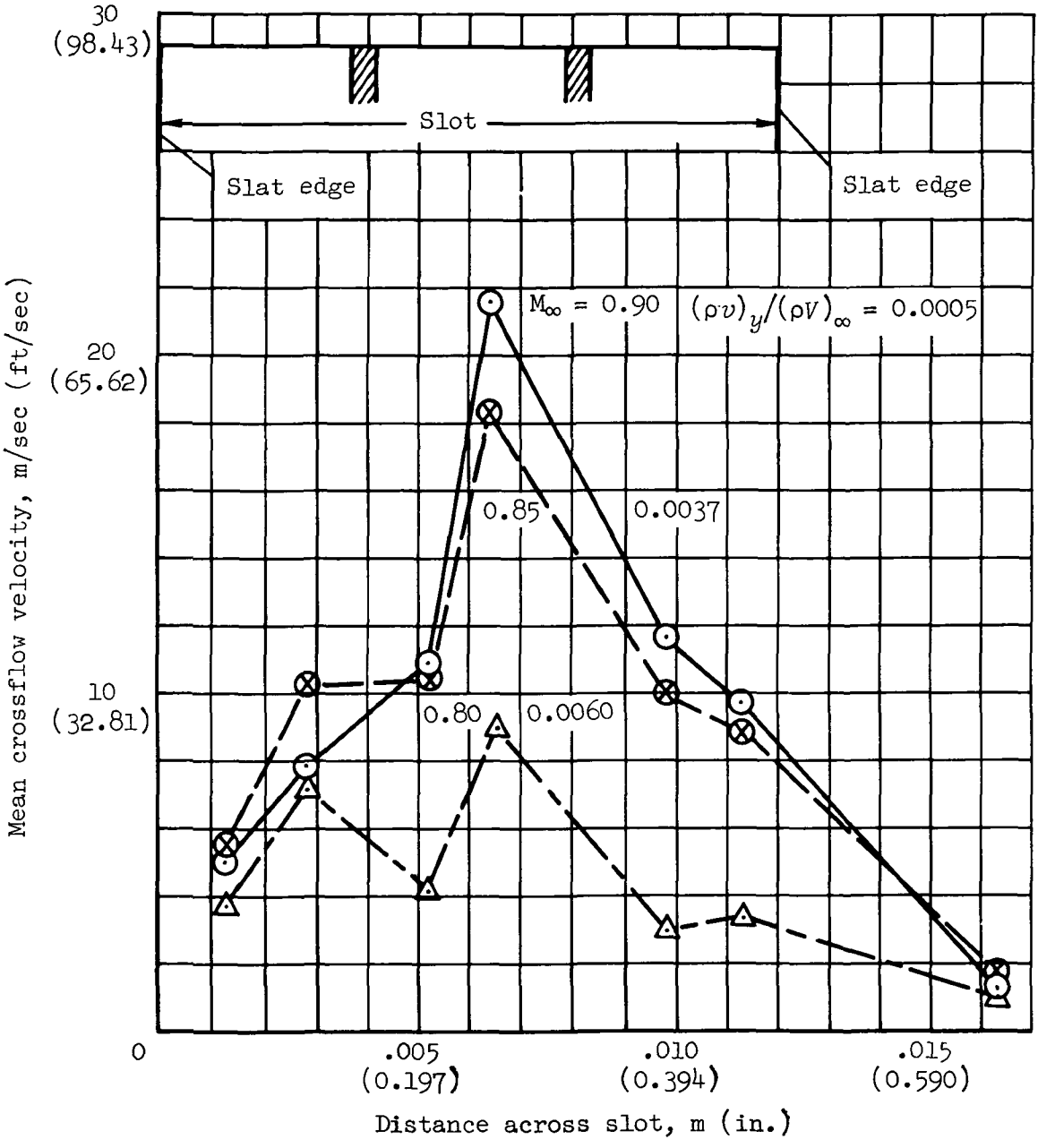

Figure 22.- Velocity distribution of crossflow across the slot exit of the 2- by 2-ft model by hot-wire measurement.

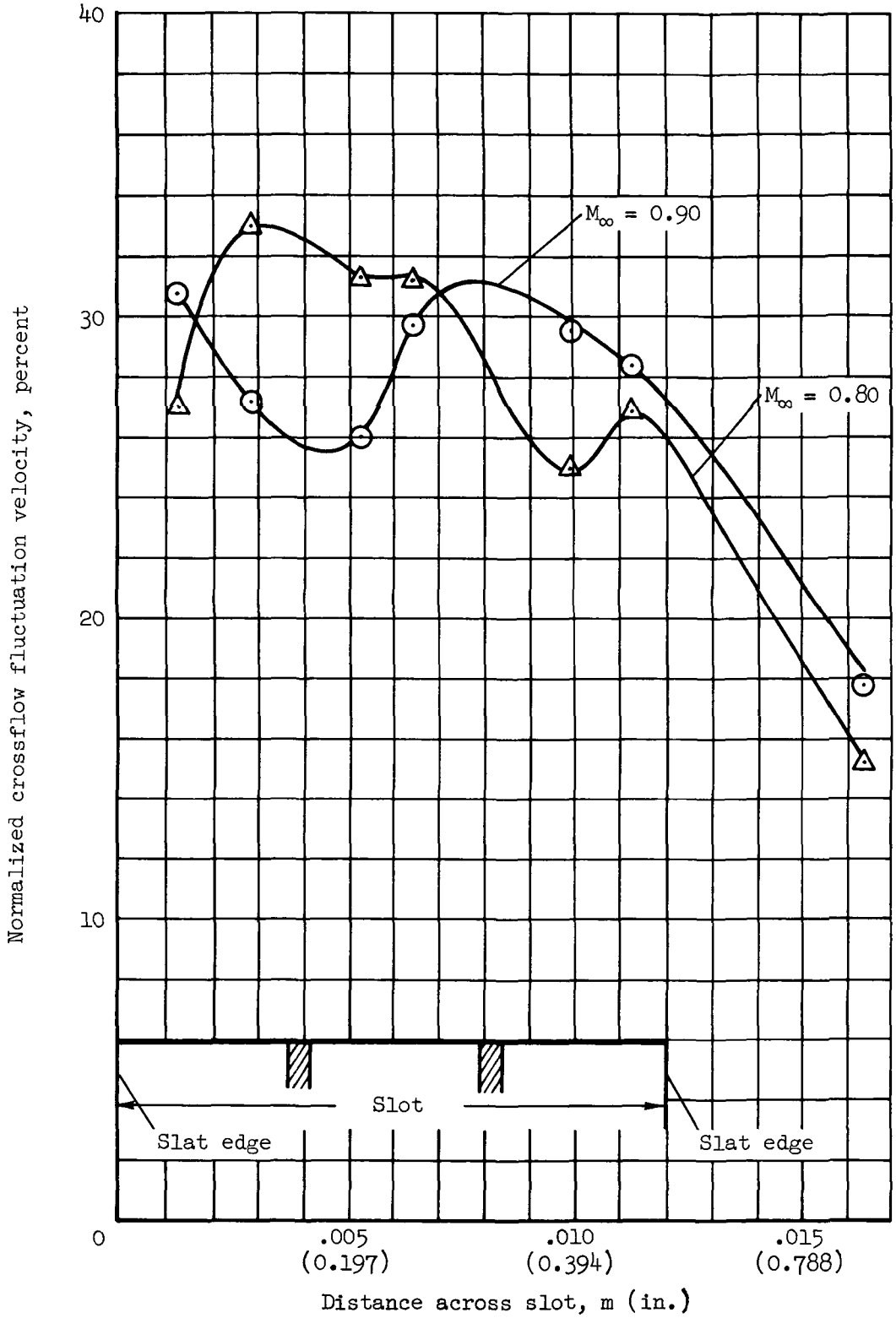

Figure 23.- Fluctuation of crossflow in the 2- by 2-ft model slot by hot-wire measurement.

1 Report No	2 Government Accession No	3. Recipient's Catalog No
NASA TM-73,257		

4 Title and Subtitle	5 Report Date
AN EXPERIMENTAL INVESTIGATION OF BOUNDARY LAYER AND CROSSFLOW CHARACTERISTICS OF THE AMES 2- BY 2-FOOT AND 11- BY 11-FOOT TRANSONIC WIND-TUNNEL WALLS	December 1977
	6 Performing Organization Code
7 Author(s)	8. Performing Organization Report No
Gerald E. Matyk* and Yasunori Kobayashi*	A-7098
	10. Work Unit No
9 Performing Organization Name and Address	505-06-42
Ames Research Center Moffett Field, California 94035	11. Contract or Grant No.
	13 Type of Report and Period Covered
12 Sponsoring Agency Name and Address	Technical Memorandum
National Aeronautics and Space Administration Washington, D. C. 20546	14 Sponsoring Agency Code

15 Supplementary Notes

*National Research Council Postdoctoral Research Associate

16 Abstract

An experimental investigation of the boundary layer and crossflow characteristics of the Ames 2- by 2-Foot and 11- by 11-Foot Transonic Wind-Tunnel wall configurations has been performed for Mach numbers ranging from 0.5 to 1.2 and for various crossflow to free-stream unit mass-flow ratios $(\rho v)_y/(\rho u)_\infty$.

For the 2- by 2-ft and 11- by 11-ft wall configurations, these ratios ranged from 0 to 0.12 and from 0 to 0.07, respectively. Most notably, for both wall configurations, the pressure-drop coefficient across the wall was nonlinear with mass flow and invariant with Mach number.

17 Key Words (Suggested by Author(s))	18 Distribution Statement
Slotted walls Tunnel walls Crossflow Wall interference	Unlimited STAR Category - 34

19 Security Classif. (of this report)	20 Security Classif (of this page)	21 No of Pages	22 Price*
Unclassified	Unclassified	40	$4.00

*For sale by the National Technical Information Service, Springfield, Virginia 22161

NASA-Langley, 1977

National Aeronautics and
Space Administration

Washington, D.C.
20546

Official Business
Penalty for Private Use, $300

THIRD-CLASS BULK RATE

Postage and Fees Paid
National Aeronautics and
Space Administration
NASA-451

U.S.MAIL

12 2 1U,D, 121277 S90844HU
MCDONNELL DOUGLAS CORP
ATTN: PUBLICATIONS GROUP, PR 15246
P O BOX 516
ST LOUIS MO 63166

NASA

POSTMASTER: If Undeliverable (Section 158 Postal Manual) Do Not Return

1-31-91 ph Roger Crites #138782 254/103/1022272/22831